



1 Measurement report: Fireworks impacts on air quality in Metro Manila, Philippines during the
2 2019 New Year revelry

3 Genevieve Rose Lorenzo^{1,2}, Paola Angela Bañaga^{2,3}, Maria Obiminda Cambaliza^{2,3}, Melliza
4 Templonuevo Cruz^{3,4}, Mojtaba AzadiAghdam⁶, Avelino Arellano¹, Grace Betito³, Rachel
5 Braun⁶, Andrea F. Corral⁶, Hossein Dadashazar⁶, Eva-Lou Edwards⁶, Edwin Eloranta⁵, Robert
6 Holz⁵, Gabrielle Leung², Lin Ma⁶, Alexander B. MacDonald⁶, James Bernard Simpas^{2,3}, Connor
7 Stahl⁶, Shane Marie Visaga^{2,3}, Armin Sorooshian^{1,6}

8 ¹Department of Hydrology and Atmospheric Sciences, University of Arizona, Tucson, Arizona,
9 85721, USA

10 ²Manila Observatory, Quezon City, 1108, Philippines

11 ³Department of Physics, School of Science and Engineering, Ateneo de Manila University,
12 Quezon City, 1108, Philippines

13 ⁴Institute of Environmental Science and Meteorology, University of the Philippines, Diliman,
14 Quezon City, 1101, Philippines

15 ⁵Space Science and Engineering Center, University of Wisconsin - Madison, Madison,
16 Wisconsin, 53706, USA

17 ⁶Department of Chemical and Environmental Engineering, University of Arizona, Tucson,
18 Arizona, 85721, USA

19 *Correspondence to: armin@email.arizona.edu*

20



21 **Abstract**

22 Fireworks degrade air quality, reduce visibility, alter atmospheric chemistry, and cause short-
23 term adverse health effects. However, there have not been any comprehensive physicochemical
24 and optical measurements of fireworks and their associated impacts in a Southeast Asia
25 megacity, where fireworks are a regular part of the culture. Size-resolved particulate matter (PM)
26 measurements were made before, during, and after New Year 2019 at the Manila Observatory in
27 Quezon City, Philippines, as part of the Cloud, Aerosol, and Monsoon Processes Philippines
28 Experiment (CAMP²Ex). A High Spectral Resolution Lidar (HSRL) recorded a substantial
29 increase in backscattered signal associated with high aerosol loading ~440 m above the surface
30 during the peak of firework activities around 00:00 (local time). This was accompanied by PM_{2.5}
31 concentrations peaking at 383.9 $\mu\text{g m}^{-3}$. During the firework event, water-soluble ions and
32 elements, which affect particle formation, growth, and fate, were mostly in the submicrometer
33 diameter range. Total (> 0.056 μm) water-soluble bulk particle mass concentrations were
34 enriched by 5.7 times during the fireworks relative to the background (i.e., average of before and
35 after the firework). The water-soluble mass fraction of PM_{2.5} increased by 18.5% above that of
36 background values. Bulk particle hygroscopicity, kappa (κ), increased from 0.11 (background) to
37 0.18 (fireworks). Potassium and non-sea salt (nss) SO₄²⁻ contributed the most (70.9%) to the
38 water-soluble mass, with their mass size distributions shifting from a smaller to a larger
39 submicrometer mode during the firework event. On the other hand, mass size distributions for
40 NO₃⁻, Cl⁻, and Mg²⁺ (21.1% mass contribution) shifted from a supermicrometer mode to a
41 submicrometer mode. Being both uninfluenced by secondary aerosol formation and constituents
42 of firework materials, a subset of species were identified as the best firework tracer species (Cu,
43 Ba, Sr, K⁺, Al, and Pb). Although these species (excluding K⁺) only contributed 2.1% of the total
44 mass concentration of water-soluble ions and elements, they exhibited the highest enrichments
45 (6.1 to 65.2) during the fireworks. Surface microscopy analysis confirmed the presence of
46 potassium/chloride-rich cubic particles along with capsule-shaped particles in firework samples.
47 The results of this study highlight how firework emissions change the physicochemical and
48 optical properties of water-soluble particles (e.g., mass size distribution, composition,
49 hygroscopicity, and aerosol backscatter), which subsequently alters the background aerosol's
50 respirability, influence on surroundings, ability to uptake gases, and viability as cloud
51 condensation nuclei (CCN).



52 **1. Introduction**

53 Fireworks affect local populations through visibility reduction and increased health risks due to
54 briefly elevated particulate matter (PM) levels. Total PM mass concentrations during local
55 celebrations in different cities have reached up to $235 \mu\text{g m}^{-3}$ (Leipzig, Germany) (Wehner et al.,
56 2000), $700 \mu\text{g m}^{-3}$ (Texas, United States [U.S.]) (Karnaee, 2005), $1,510 \mu\text{g m}^{-3}$ (Montreal,
57 Canada) (Joly et al., 2010), and $2,582 \mu\text{g m}^{-3}$ (New Delhi, India) (Mönkkönen et al., 2004).
58 These levels exceed the 24 h U.S. National Ambient Air Quality Standard (NAAQS) for PM_{10} of
59 $150 \mu\text{g m}^{-3}$. Firework emissions from at least nineteen studies have also been linked to
60 exceedance of the 24 h U.S. NAAQS limit for $\text{PM}_{2.5}$ of $35 \mu\text{g m}^{-3}$ (Lin, 2016 and references
61 therein). Higher PM concentrations from fireworks have been reported more frequently in Asia
62 (i.e., India, China, and Taiwan) compared to Western countries (Lin, 2016; Sarkar et al., 2010).

63 Health effects are of major concern during firework periods based on both short and long-term
64 exposure. For example, Diwali is a major firework festival in India where it was shown that
65 chronic exposure to three of the most prominent tracer species (Sr, K, and Ba) translated to a 2%
66 increase in health effects based on the non-carcinogenic hazard index (Sarkar et al., 2010). On
67 the other hand, short term exposure to firework pollutants increases asthma risk, eye allergies,
68 cardiovascular and pulmonary issues, cough, and fever (Moreno et al., 2010; Singh et al., 2019;
69 Barman et al., 2008; Becker et al., 2000; Beig et al., 2013; Hirai et al., 2000). Firework pollutants
70 also impact clouds and the hydrological cycle, owing to associated aerosols serving as cloud
71 condensation nuclei (CCN) (Drewnick et al., 2006) and subsequently impacting surface
72 ecosystems after wet deposition (Wilkin et al., 2007). Although fireworks emit particles with
73 various sizes into the atmosphere, fine particles associated with $\text{PM}_{2.5}$ are most relevant to public
74 health effects, scattering efficiency, and CCN activation (Vecchi et al., 2008; Perry, 1999).
75 Knowing the various effects of firework emissions depends on knowing their physical, chemical,
76 and optical properties.

77 Measurements of the chemical composition of firework emissions are important in order to
78 understand how they affect local air quality. The main components of fireworks are fuels (metals
79 and alloys, metalloids, and non-metals), oxidizers (nitrates, perchlorates, and chlorates), and
80 coloring agents (metal salts) (Steinhauser and Klapotke, 2010). Previous studies have relied on
81 tracer species to establish confidence in distinguishing the firework source from background air
82 and other sources (Sarkar et al., 2010). Potassium historically has been the most observable
83 tracer for fireworks emissions (Wang et al., 2007; Drewnick et al., 2006; Perry, 1999), with
84 concentrations reaching $58 \mu\text{g m}^{-3}$ during the Diwali Festival in India (Kulshrestha et al., 2004).
85 Firework color is created by metal salts such as Sr for red, Ba for green, and Cu for blue, all
86 three of which have and have been found to be effective tracers of fireworks (Walsh et al., 2009;
87 Vecchi et al., 2008). Strontium in particular is an indicator of the spatial and temporal extent of
88 firework smoke plumes (Perry, 1999) because of the high prevalence of red in fireworks and it is
89 not affected by traffic emissions (Moreno et al., 2010). Other components measured in the air that
90 have been attributed to fireworks include metals such as Al, Cd, Cu, Ti, Mg, Mn, Ni, Zn, their
91 salt anion counterparts (S, P, Cl) and other trace metals (As, Bi, Co, Ga, Hg, Cr, Pb, Rb, Sb, and
92 P). Also from fuel and oxidizer combustion are species such as NO_3^- , SO_4^{2-} , and organics
93 including oxaloacetic acid (Alpert and Hopke, 1981; Barman et al., 2008; Carranza et al., 2001;



94 Dorado et al., 2001; Drewnick et al., 2006; Joly et al., 2010; Joshi et al., 2016; Kulshrestha et al.,
95 2004; Kumar et al., 2016; Lin et al., 2016; Moreno et al., 2010; Sarkar et al., 2010; Tanda et al.,
96 2019; Thakur et al., 2010; Joshi et al., 2019). Black carbon mass concentrations during firework
97 events can either increase due to firework emissions or decrease owing to fewer vehicles on the
98 road (Kumar et al., 2016; Yadav et al., 2019). In both cases, the black carbon mass fraction
99 decreases due to a greater contribution of other constituents in firework emissions. Organic mass
100 concentrations and mass fractions have been noted to increase and decrease, respectively, with
101 fireworks (Zhang et al., 2019). Governed largely by composition, particulate hygroscopicity and
102 solubility have also been found to be altered by fireworks depending on the emitted species.
103 Copper and Mg were observed to become more soluble in firework emissions in Delhi, India,
104 while Mn, As, Ba, and Pb became less soluble (Perrino et al., 2011). The water-soluble aerosol
105 component from fireworks in Sichuan Basin (China) were internally mixed and enhanced the
106 hygroscopicity of submicrometer aerosols, especially the larger particles (Yuan et al., 2020).

107 In addition to composition, a necessary aspect of characterizing impacts of firework emissions is
108 to measure aerosol size distributions within the short timeframe of an event (Joshi et al., 2019).
109 Owing to combustion during firework events, PM concentrations are dominated by particles in
110 the submicrometer range (Vecchi et al., 2008; Nicolás et al., 2009; Joshi et al., 2019; Pirker et
111 al., 2020; Do et al., 2012). Particle number concentration maxima have been noted for the
112 nucleation (0.01 to 0.02 μm) and Aitken (0.02 to 0.05 μm) modes (Yadav et al., 2019; Yuan et
113 al., 2020), in addition to both the small (0.1 to 0.5 μm) (Wehner et al., 2000; Zhang et al., 2010)
114 and large (0.5 to 1.0 μm) ends of the accumulation mode (Vecchi et al., 2008) during firework
115 events. There are a few studies with observed particle mass concentration increases in the coarser
116 but still respirable ($< 10 \mu\text{m}$) mode (Tsai et al., 2011). In terms of dynamic behavior in the size
117 distributions, past work has shown a shift in number concentration from nucleation and Aitken
118 modes to the smaller end of the accumulation mode (0.1 to 0.5 μm), due to increased coagulation
119 sinks (Zhang et al., 2010). Finer temporal scale monitoring has revealed steep increases in
120 nucleation mode and Aitken mode particle concentrations associated with firework emissions
121 followed by a growth in accumulation mode particle number concentrations due to coagulation
122 (Yadav et al., 2019). An opposite shift to a smaller size distribution has been observed for certain
123 species (Mg, Al, Cu, Sr, and Ba) from the coarse mode to accumulation mode (Tanda et al.,
124 2019). Other work has shown that while there is usually a quick drop in particle concentration to
125 background values after firework events (Joly et al., 2010), elevated number concentrations of
126 accumulation mode particles are maintained for up to three hours after peak firework activity
127 (Hussein et al., 2005). New particle formation events with fireworks have also been reported in
128 Mumbai, India (Joshi et al., 2016), with enrichments of primary and secondary particles for up to
129 30 minutes after peak firework activity. Particle aging due to distance from the source and
130 meteorology alter firework emission particle concentrations (Joly et al., 2010) and size
131 distributions (Khaparde et al., 2012).

132 Meteorological and dynamic parameters such as wind speed, level of mixing (turbulent kinetic
133 energy), and mixing layer height (Lai and Brimblecombe, 2020) influence peak concentration
134 and composition of aerosols after fireworks, as well as particle residence time in the atmosphere



135 and transport to nearby regions (Vecchi et al., 2008). Although firework activities are episodic,
136 their particulate emissions, especially in the submicrometer mode (Do et al., 2012), reside in the
137 atmosphere for as long as several days to weeks (Liu et al., 1997; Lin et al., 2016; Kong et al.,
138 2015; Do et al., 2012). Dispersion of the particles under low wind speed (1 m s^{-1}) for particles
139 between 0.4 and 1 μm is estimated at 12 h (Vecchi et al., 2008) and can reach distances as far as
140 a hundred kilometers (Perry, 1999). Aitken mode and larger particles are dispersed by wind more
141 than nucleation-mode particles (Agus et al., 2008). Meteorological conditions, such as rainfall,
142 can also decrease firework particle loading in the air and relative humidity can change the
143 hygroscopicity of firework emissions (Hussein et al., 2005), thereby affecting their size and
144 radiative properties.

145 There currently is no in-depth analysis of the chemical, physical, and optical properties of
146 firework emissions in a Southeast Asian megacity where fireworks are culturally significant. This
147 work reports on size-resolved aerosol characteristics during the 2019 New Year celebrations in
148 Metro Manila, Philippines, one of the most populated cities, with 12.88 M population (PSA,
149 2015), in Southeast Asia. We address the following questions in order: (i) what is the
150 meteorological backdrop during the study period in relation to $\text{PM}_{2.5}$ levels; (ii) what is the effect
151 of the firework emissions on optical properties of aerosols?; (iii) what are the concentrations and
152 mass size distribution characteristics of different elemental and ionic species?; (iv) what are the
153 most enhanced tracers in firework emissions?; (v) what are the size-resolved morphological
154 characteristics of firework aerosols?; (vi) how does aerosol hygroscopicity respond to firework
155 emissions? The results of this work provide new data that can help address how past and on-
156 going firework emissions impact health, visibility, regional air quality, and biogeochemical
157 cycling of nutrients and contaminants in the Philippines, Southeast Asia, and, more broadly, for
158 all other cities with major firework events. It also contributes to the growing body of firework
159 research findings (Devara et al., 2015), with a unique feature of this work being the combination
160 of multiple data products, including surface-based lidar retrievals and size-resolved composition
161 and morphology analyses. Firework events are widespread episodes that can also be used to
162 expose and ultimately resolve differences between satellite and surface data (Williams et al.,
163 2005; Kumar et al., 2016).

164
165 **2. Methods**

166 **2.1 Hourly $\text{PM}_{2.5}$ Mass Concentration**

167 Hourly $\text{PM}_{2.5}$ mass concentrations were obtained to assess temporal characteristics of fine
168 particulates due to fireworks and their relation to meteorology and aerosol optical properties. The
169 hourly $\text{PM}_{2.5}$ mass concentrations were collected at the Manila Observatory, Quezon City,
170 Philippines (14.64°N , 121.08°E , ~70 m. a. s. l.) (Fig. S1) with a beta attenuation monitor
171 (DKK-TOA Corporation) as part of the East Asia Acid Deposition Monitoring Network
172 (EANET) (Totsuka et al., 2005). The beta attenuation monitor collects $\text{PM}_{2.5}$ samples on a ribbon
173 filter, which are irradiated with beta particles. The attenuation of the beta particles through the
174 sample and the filter is exponentially proportional to the mass loading on the filter. These hourly



175 data were then averaged over 48-hour periods coinciding with water-soluble aerosol composition
176 measurements (Section 2.4) before, during, and after the firework event.

177

178 2.2 Meteorological Data

179 Rainfall, temperature, relative humidity, and wind data were collected at the Manila Observatory
180 with a Davis Vantage Pro2 Plus weather station (~90 m. a. s. l) before, during, and after the
181 firework period. Hourly precipitation accumulation and 10-min averaged temperature, relative
182 humidity, and wind were used for the analysis.

183

184 2.3 Remote Sensing

185 Vertical profiles of aerosol backscatter cross-section measured with the University of Wisconsin
186 High Spectral Resolution Lidar (HSRL) which was deployed at the Manila Observatory in
187 support of CAMP²EX. The HSRL instrument transmitting laser (Table S1) operates at 532 nm
188 with 250 mW average power and pulse repetition rate of 4 KHz. The HSRL technique measures
189 and separates the returned signal into the molecular and aerosol backscatter by using a beam
190 splitter and an iodine absorption cell filter. The separated molecular signal allows for optical
191 depth and backscatter cross section measurements in contrast to a standard backscatter lidar that
192 requires assumption related to the particulate lidar ratio (Razenkov, 2010). The HSRL also
193 measures particulate depolarization ratio, an indicator of aerosol or cloud particle shape with low
194 depolarization indicative of spherical particles while intermediate values (10%) indicate a mix of
195 spherical and nonspherical particles (Burton et al., 2014; Reid et al., 2017). HSRL data were
196 uploaded and processed at the University of Wisconsin-Madison Space Science and Engineering
197 Center server for periods before, during, and after the fireworks.

198

199 2.4 Aerosol Composition and Morphology Measurements

200 Size-specified PM (cut-point diameters: 18, 10, 5.6, 3.2, 1.8, 1.0, 0.56, 0.32, 0.18, 0.10, and
201 0.056 μm) was collected on Teflon substrates (PTFE membrane, 2 μm pores, 46.2 mm diameter,
202 Whatman) with two Micro-Orifice Uniform Deposition Impactor (MOUDI II 120R, MSP
203 Corporation) (Marple et al., 2014) samplers from the third floor of the main building (~85 m. a.
204 s. l) at the Manila Observatory. Sample collection for each of the three MOUDI sets lasted 48
205 hours before (13:30 December 24, 2018 to 13:30 December 26, 2018), during (14:45 December
206 31, 2018 to 14:45 January 2, 2019), and after (13:30 January 1, 2019 to 13:30 January 3, 2019)
207 firework activities. Note all times refer to local time (UT + 8 hours). Although there were no
208 fireworks released from the sampling site, there was firework activity in the immediate vicinity
209 (~ 500 m from the sampling in all directions and all throughout the city in general). Firework
210 activity around the sampling site began around ~19:00 on December 31, 2018 and peaked at
211 00:00 of 1 January 2019). There was limited firework after midnight. MOUDI samples collected
212 before and after the firework event were considered as background samples. Although there is



213 some firework activity that is expected in the evening of December 24 (before the firework
214 event), this is minimal compared to that which is the focus of this study. The samples were
215 covered with aluminum foil, sealed, and stored in the freezer before being shipped to the
216 University of Arizona for elemental and ionic analysis.

217 Each sample substrate was cut in half. One half of each sample was extracted in 8 mL Milli-Q
218 water (18.2 MΩcm), sonicated, and analyzed for ions (ion chromatography (IC): Thermo
219 Scientific Dionex ICS-2100 system) and elements (triple quadrupole inductively coupled plasma
220 mass spectrometer: ICP-QQQ; Agilent 8800 Series). The remaining substrate halves were stored.
221 Sample ionic and elemental concentrations were corrected by subtracting concentrations from
222 background control samples. More information about the sampling and analysis are detailed in
223 recent work (Stahl et al., 2020b). Limits of detection of the forty-one reported species are
224 summarized in Table S3. Potassium (K^+) was reported based on ICP-QQQ measurements rather
225 than IC due to possible contamination from the KOH eluent used in the latter instrument. Non-
226 sea salt SO_4^{2-} was calculated by subtracting $0.2517 * Na^+$ from the total SO_4^{2-} concentration
227 (Prospero et al., 2003).

228 High-resolution scanning electron microscopy (SEM) combined with energy dispersive X-ray
229 analysis (EDX) was used for examining particle morphology and chemical composition on a
230 portion of the substrates collected during the firework event. Analyses were performed with a
231 Hitachi S-4800 high-resolution SEM and a Thermo Fisher Scientific Noran Six X-ray
232 Microanalysis System in the Kuiper Imaging cores at the University of Arizona. Approximately
233 1 cm^2 was cut from the center of substrate halves and placed on double-sided carbon tape
234 mounted on an aluminum stub. A thin layer (1.38 nm) of carbon was coated on the sample
235 surface using a Leica EM ACE600 sputter coater to improve the sample's conductivity. SEM
236 images were obtained at 15 keV and 30 keV acceleration voltages and with a 20 μA probe
237 current in high-magnification mode. The percentage contributions and the spatial distribution of
238 the elements were obtained from the EDX analysis. Carbon, F, and Al should be ignored in the
239 discussion of SEM-EDX results since C and F are present in the Teflon substrates, and the
240 sample stub is an Al-rich substrate.

241

242 2.5 Enrichment Factor Calculations

243 To identify which species are most enhanced during fireworks, enrichment values are typically
244 calculated using speciated concentrations during the fireworks relative to baseline periods
245 (Tanda et al., 2019). We calculate water-soluble mass enrichment factors for each of the forty-
246 one measured species by dividing their total bulk ($\geq 0.056 \mu m$) mass concentrations during the
247 firework event by the average of the total mass concentration of the species measured before and
248 after the firework event. Size-resolved enrichments were similarly calculated using measured
249 mass concentrations for individual MOUDI stages. In a case when the mass concentration of a
250 species during the firework event was non-zero but the mass concentrations during and after
251 were zero (e.g., succinate), half of the detection limit was used in place of zero values.

252



253 2.6 Hygroscopicity Calculations

254 Hygroscopicity was calculated for particles ranging in size between 0.056 – 3.2 μm before,
255 during, and after the firework event. This size range was chosen to most closely be aligned with
256 separate measurements of $\text{PM}_{2.5}$ in the study (Section 2.1) that were used to account for the
257 remaining mass not speciated in this study. We specifically calculate values for the single
258 hygroscopicity parameter κ (Petters and Kreidenweis, 2007).

259 The water-soluble compound mass concentrations before, during, and after the firework event
260 were calculated using an ion-pairing scheme (Gysel et al., 2007) for each MOUDI stage between
261 diameters of 0.056 and 3.2 μm , and then summed to achieve a total mass concentration for each
262 compound in this size range. Black carbon mass concentrations in $\text{PM}_{2.5}$ before and after the
263 firework event were calculated based on their long-term (2001-2007) average contribution (32%)
264 to $\text{PM}_{2.5}$ mass in December and January (Cohen et al., 2009). Black carbon or elemental carbon
265 (EC) concentrations during the firework event were assumed to be the average of the black
266 carbon concentrations before and after the firework event. This was done because black carbon
267 concentrations have been observed to not increase (Santos et al., 2007) as much as organic
268 carbon (OC) (Lin, 2016), such that OC:EC mass ratios during fireworks have been observed to
269 increase. Total non-water-soluble content between 0.056 and 3.2 μm was calculated as the
270 difference between the total $\text{PM}_{2.5}$ mass concentration and the sum of the water-soluble species
271 and black carbon mass concentrations. The mass of each species was divided by its density, and
272 each of these volumes were added to quantify the volume of the measured aerosol (water-soluble
273 compounds, black carbon, and organic matter) between 0.056 and 3.2 μm . Volume fractions
274 were then computed for each species. The Zdanovskii, Stokes, and Robinson (ZSR) mixing rule
275 (Stokes and Robinson, 1966) was used to obtain the total hygroscopicity (total κ) of the mixed
276 aerosols by weighting κ values for the individual non-interacting compounds by their respective
277 volume fractions and summing linearly. Densities and κ values for the individual compounds are
278 based on those used elsewhere (AzadiAghdam et al., 2019), repeated in Table S4.
279

280 2.7 Back Trajectories

281 Three-day back trajectories with six-hour resolution were generated using the National Oceanic
282 and Atmospheric Administration's (NOAA) Hybrid Single-Particle Lagrangian Integrated
283 Trajectory (HYSPLIT) model (Rolph et al., 2017; Stein et al., 2015) using the Global Data
284 Assimilation System (GDAS) with a resolution of 1°, and vertical wind setting of “model vertical
285 velocity”. Back trajectories were chosen to end at the beginning times of the sampling periods
286 before, during, and after the firework event. Trajectories were computed for an end point being at
287 the Manila Observatory at an altitude of 500 m because it represents the mixed layer as done in
288 other works examining surface air quality (Mora et al., 2017; Aldhaif et al., 2020; Crosbie et al.,
289 2014; Schlosser et al., 2017).
290

291 **3. Results and Discussion**



292 3.1 Hourly PM_{2.5}, Meteorological, and Transport Patterns

293 Temporal analysis of PM_{2.5} and meteorology (Fig. 1) can help in understanding how the
294 enhanced particulate concentrations detected at the Manila Observatory during the fireworks
295 evolved and were influenced by meteorology. Hourly PM_{2.5} began to increase from 44.0 $\mu\text{g m}^{-3}$
296 (shortly after rising above the 24-h Philippine National Ambient Air Quality Guideline Value
297 (NAAQGV) of 50.0 $\mu\text{g m}^{-3}$) after 18:00 on 31 December 2018 with the beginning of firework
298 activity and calm meteorological conditions. There was moderate (3 mm) rainfall from 22:00 to
299 23:00 that night as the firework activity began to increase. Rain is a sink for particles (Perry,
300 1999) and could have washed out some of the particulates in the air, thus potentially causing a
301 slight dip in the hourly PM_{2.5} around midnight. PM_{2.5} peaked at 383.9 $\mu\text{g m}^{-3}$ between 01:00 to
302 02:00 on 1 January 2019. The PM_{2.5} peak was delayed by approximately an hour from the peak
303 firework activity at midnight possibly due to rainfall, relative humidity, and wind (Vecchi et al.,
304 2008), in addition to aerosol dynamical processes requiring time for secondary aerosol formation
305 and growth (Li et al., 2017). Minimal rain (0.2 mm in an hour) with high relative humidity
306 (between 93% \pm 4% to 94% \pm 4%) were conducive to aerosol growth and/or secondary particle
307 formation. High relative humidity is related to aqueous-phase oxidation of SO₂ (Sun et al., 2013)
308 and NO₂ (Cheng et al., 2014) as well as metal-catalyzed heterogeneous reactions (Wang et al.,
309 2007) to form SO₄²⁻. Aqueous oxidation has been found to be a predominant mechanism for the
310 secondary formation of SO₄²⁻ during fireworks (Li et al., 2017), in addition to promoting
311 secondary organic aerosol formation (Wonaschuetz et al., 2012; Youn et al., 2013). Light wind
312 (\sim 1 m s⁻¹) after midnight from the northeast could also have transported more emissions from the
313 populated Marikina Valley, located in the northeast, to the Manila Observatory contributing to
314 the delay of the PM_{2.5} peak.

315 Particulate levels were enhanced for approximately 14 h from the beginning of the firework
316 activity (Fig. 1) during which the average PM_{2.5} (143.4 $\mu\text{g m}^{-3}$) exceeded the 24 h Philippine
317 NAAQGV between 18:00 on 31 December 2018 to 08:00 on 1 January 2019. After 02:00 on 1
318 January 2019, PM_{2.5} dropped quickly to 122.0 $\mu\text{g m}^{-3}$ between 03:00 to 04:00 (Fig. 1). The PM_{2.5}
319 decrease was less pronounced after 04:00 but continued decreasing steadily along with slight rain
320 (0.4 mm in an hour) and light breeze (1 – 2 m s⁻¹) from the northwest to southwest directions.
321 Firework activity in other countries have been documented to last from 2 – 6 h in a day and
322 elevated particulate levels can be maintained for up to 6 – 18 h (Thakur et al., 2010; Crespo et
323 al., 2012; Chatterjee et al., 2013; Kong et al., 2015; Tsai et al., 2012). The 48-h average PM_{2.5}
324 during (49.9 $\mu\text{g m}^{-3}$) the firework event was 1.9 and 3.3 times more, respectively, than before
325 (25.8 $\mu\text{g m}^{-3}$) (Fig. S2) and after (15.2 $\mu\text{g m}^{-3}$) (Fig. S3) the firework event. Previous work in
326 other countries has shown two to three-fold increases in PM due to fireworks (Rao et al., 2012;
327 Ravindra et al., 2003; Tsai et al., 2011; Shen et al., 2009). Greater increases (> 5 times) in
328 particulate levels elsewhere were related to more intense and prolonged (days) firework activity
329 (Tian et al., 2014).

330 Air parcel trajectories arriving at the Manila Observatory during the sampling periods before,
331 during, and after the firework event were assessed to ascertain the impact of fireworks on the



332 enhanced particulate concentrations. Three-day back trajectories for the period before the
333 firework event were from the northeast to east directions coming from the Philippine Sea (Fig.
334 2a). For the periods (Fig. 2b) during and (Fig. 2c) after the firework event, back trajectories were
335 from the northeast to east/northeast directions. The general wind directions from the back
336 trajectories are consistent with the climatologically prevailing northeasterly monsoonal winds in
337 December and January for the Philippines (Villafuerte II et al., 2014). The origin of the air
338 parcels did not have any major emissions events that could have impacted the measurements
339 after long-range transport. This is important to note because the tracers for fireworks are also
340 tracers for transported emissions due to biomass burning (K^+) (Braun et al., 2020) and industrial
341 activities (Cohen et al., 2009). Thus, enriched particulate concentrations during the firework
342 activity were most likely locally produced.

343

344 3.2 Optical Aerosol Properties

345 Heavy aerosol loading at the surface was observed up to eight hours after the fireworks peak (16
346 UTC, 12 AM local time) with high HSRL 532 nm backscatter cross-section and depolarization
347 (Fig. 3a) reaching ~440 m above the ground. Prior to the firework peak, the surface aerosol layer
348 had lower backscatter (before 14 UTC, Fig. 3a), and this cleaner condition is shown by the 08:16
349 UTC vertical profile of the aerosol backscatter (Fig. 3b). Rainfall (Fig. 1a) contributed to
350 columns of high backscatter (Fig. 3a) after 14 UTC and before the firework peak with a
351 measurable decrease in the aerosol backscatter for a short time after the precipitation (15:00 and
352 16:00 UTC).

353 To verify the height values (Fig. 3b), the “surface-attached aerosol layer” height is estimated
354 using the maximum variance method more commonly used for daytime convective boundary
355 layer detection (Hooper and Eloranta, 1986). The method is also limited by the complexity of the
356 case due to pertinent rain signals for this event. The “surface attached aerosol layer” (Fig. 3a) is
357 derived from a 15-min moving window average based on the 30-s values shown with a thin black
358 line. As confirmed by the height detection, aerosols reached up to ~440 m (Fig 3a and b) on 16
359 UTC (31 December 2018). It persisted for at least an hour then dropped to 118 ± 20 m with
360 higher aerosol backscatter retained until January 1, 2019 0 UTC. Some of the smoke is above the
361 detected height (i.e. 17 UTC).

362

363 3.3 Mass Size Distributions

364 A total of 41 water-soluble species were detected in the 48-hr size-differentiated particulate
365 samples collected before, during, and after the firework event. The total bulk mass concentration
366 is defined as the sum of the concentrations of all the measured species across the MOUDI’s
367 eleven stages ($\geq 0.056 \mu\text{m}$). The total water-soluble bulk mass concentration (Table 1) during the
368 firework event ($16.74 \mu\text{g m}^{-3}$) was 5.71 times and 4.73 times higher than the total bulk mass



369 concentrations before ($2.93 \mu\text{g m}^{-3}$) and after ($3.54 \mu\text{g m}^{-3}$) the firework event, respectively.
370 Assuming the average of the water-soluble mass concentrations before and after the firework
371 event represent background values, this translates to an 80.66% increase in water-soluble mass
372 during the firework event.

373 The firework event was associated with increased total water-soluble mass fraction (32.33%)
374 (0.056 – $3.2 \mu\text{m}$ size range, Section 3.1) in $\text{PM}_{2.5}$ (Fig. S4) compared to before (9.90%) and after
375 (17.79%) the firework event. The water-soluble particulate mass fraction in $\text{PM}_{2.5}$ similarly
376 increased in other firework events (Yang et al., 2014). The highest total water-soluble mass
377 concentrations during the firework event were from the following ions: non-sea salt (nss) SO_4^{2-}
378 ($6.81 \mu\text{g m}^{-3}$), K^+ ($5.05 \mu\text{g m}^{-3}$), NO_3^- ($1.70 \mu\text{g m}^{-3}$), Cl^- ($1.46 \mu\text{g m}^{-3}$), Mg^{2+} ($0.37 \mu\text{g m}^{-3}$), Na^+
379 ($0.33 \mu\text{g m}^{-3}$), and Ca^{2+} ($0.30 \mu\text{g m}^{-3}$). These contributed to 95.75% of the total detected bulk
380 water-soluble mass concentration then.

381 Total water-soluble bulk mass concentration during the firework event was dominated by
382 submicrometer particles, which accounted for 77.4% of the total water-soluble bulk mass (Fig.
383 4b). Supermicrometer mass fractions were greater before (Fig. 4a) and after (Fig. 4c) the
384 firework event (43.7% and 57.5% of the water-soluble bulk mass concentration) compared to
385 during the firework event (22.6%). The increase in submicrometer mass fractions is typical with
386 firework emissions (Crespo et al., 2012; Do et al., 2012). In New York, fireworks contributed to
387 77% of PM_1 due to potassium salts and oxidized organic aerosol (Zhang et al., 2019).

388 Non-sea salt SO_4^{2-} had the highest contribution (40.7%) to total water-soluble bulk mass
389 concentration during the firework event (Table 1). Sulfate exhibited a shift in its mass size
390 distribution to a slightly larger size during firework activity (Fig. 4b). During the firework event,
391 87.13 % of the nss- SO_4^{2-} was in the $0.32 \mu\text{m}$ to $1.8 \mu\text{m}$ size fraction. Before and after the
392 firework event, 87.28% and 85.14% of the nss- SO_4^{2-} mass concentration, respectively, was
393 distributed in a finer size fraction ($0.18 \mu\text{m}$ to $1 \mu\text{m}$) (Fig. 4a and 4c). For context, SO_4^{2-} peaked
394 at $0.62 \mu\text{m}$ during fireworks in Nanning, China (Li et al., 2017). Firework emissions include
395 gases like SO_2 which undergo aqueous uptake and oxidation onto particles to form SO_4^{2-} .
396 Furthermore, enhanced secondary formation is aided by metals emitted during fireworks that
397 help convert SO_2 to SO_4^{2-} (Feng et al., 2012; Wang et al., 2007).

398 Potassium contributed 30.19% to the total water-soluble mass concentration during the firework
399 event (Table 1), presumably in the form of KNO_3 . This compound is associated with black
400 powder used as a propellant (Li et al., 2017). Potassium's mass concentration distribution
401 similarly shifted to a slightly larger size during the firework event (Figure 4b). Most (87.6%) of
402 the bulk K^+ mass concentration during the firework event was between 0.32 and $1.8 \mu\text{m}$,
403 compared to 85.4% and 79.4% between 0.18 and $1 \mu\text{m}$ before and after the firework event,
404 respectively (Fig. 4a and 4c). This is comparable to the mass diameter ($0.7 \mu\text{m}$) due to firework
405 emissions after transport in Washington State (Perry, 1999). The shift in the mass size
406 distribution of K^+ and nss- SO_4^{2-} can be due to the removal of nucleation-mode particles as a
407 result of increased coagulation in the accumulation mode (Zhang et al., 2010).



408 Nitrate, Cl^- , and Mg^{2+} mass size distributions all exhibited pronounced peaks in the
409 submicrometer range during the firework event (Fig. 5). The mass sum concentration of the
410 aforementioned ions peaked (46.39% of the total mass concentration of the three species)
411 between 0.56 and 1.0 μm . On the other hand, their mode appeared between 1.8 and 3.2 μm
412 before and after the firework event (33.02% and 32.91% of the total mass concentration of the
413 three species, respectively) (Fig. 5). Nitrate, Cl^- , and Mg^{2+} are emitted during fireworks (Zhang et
414 al., 2017) as finer-sized submicrometer particles (Tsai et al., 2011) compared to background
415 conditions when these species are mostly associated with coarser supermicrometer particles
416 (AzadiAghdam et al., 2019; Cruz et al., 2019; Hilario et al., 2020). Nitrate can also be formed
417 secondarily (Yang et al., 2014) from firework emissions. Firework emissions are associated with
418 lower $\text{NO}_3^-:\text{SO}_4^{2-}$ ratios (Feng et al., 2012) compared to days dominated by mobile sources
419 (Arimoto et al., 1996) due to different formation mechanisms (Tian et al., 2014). Consistent with
420 the literature, low $\text{NO}_3^-:\text{SO}_4^{2-}$ ratios were also observed during the firework event (before: 0.79,
421 during: 0.25, after: 0.82). A low $\text{NO}_3^-:\text{SO}_4^{2-}$ ratio is related to decreased pH of the particles (Cao
422 et al., 2020), which may impact not just air quality and health but also nearby waterbodies where
423 the particles may deposit. It is important to note that background supermicrometer Cl^- and Mg^{2+}
424 in Manila are most likely associated with sea salt while background supermicrometer NO_3^-
425 possibly in the form of NaNO_3 (de Leeuw et al., 2001) or NH_4NO_3 likely stems from partitioning
426 of nitric acid gas onto surfaces (de Leeuw et al., 2001) of coarse particles such as sea salt and
427 dust (AzadiAghdam et al., 2019; Cruz et al., 2019). The $\text{Cl}^-:\text{Na}^+$ mass ratio during the firework
428 event increased to 4.44 (from 0.69 and 1.08 before and after, respectively) and was higher than
429 the typical $\text{Cl}^-:\text{Na}^+$ ratio in seawater of 1.81 (Braun et al., 2017). These ratio results confirm that
430 the increase in Cl^- concentrations during the firework event is not driven by sea salt but instead
431 linked to firework emissions such as what was shown during Taiwan's lantern festival with $\text{Cl}^-:\text{Na}^+$
432 ratios reaching approximately 3 owing to raw materials in fireworks such as KClO_3 , ClO_3 , and
433 ClO_4 (Tsai et al., 2012). The lack of increased sea salt influence during the firework event,
434 which is not to be expected, is further confirmed by relatively small changes in the amount of
435 observed Na^+ , as will be discussed subsequently.

436 The Na^+ , Ca^{2+} , and NH_4^+ mass size distributions peak in the supermicrometer range (1.8 to 3.2
437 μm) (Figure S5) and total mass concentrations (Table 1) varied minimally, relative to the earlier
438 mentioned species, before (0.33 $\mu\text{g m}^{-3}$, 0.21 $\mu\text{g m}^{-3}$, 0.21 $\mu\text{g m}^{-3}$, respectively), during (0.33 μg
439 $\mu\text{g m}^{-3}$, 0.30 $\mu\text{g m}^{-3}$, 0.19 $\mu\text{g m}^{-3}$) and after (0.53 $\mu\text{g m}^{-3}$, 0.38 $\mu\text{g m}^{-3}$, 0.28 $\mu\text{g m}^{-3}$) the firework
440 event. The minimal change in NH_4^+ mass concentration is most likely due to little or no variation
441 of its precursor gas (e.g., NH_3) due to firework activities and the fact that firework materials are
442 commonly composed of K-rich salts rather than NH_4^+ salts (Zhang et al., 2019). The latter seems
443 probable because the K:S mass ratios of 2.75 and 2.71, observed from 0.18 – 0.32 μm and 0.32 –
444 0.56 μm , respectively, during the firework event suggests a firework-related source of K and S.
445 This ratio is similar to the K:S ratio of 2.75 (Dutcher et al., 1999) of “black powder” (Perry,
446 1999), a type of pyrotechnic comprised of K and S.



447 The mass size distribution for the sum of the rest of the species (“others” in Fig. 4) shifted from
448 having a peak at the smaller end of the accumulation mode (0.18 – 0.32 μm) before and after the
449 firework event to larger sizes in the accumulation mode (0.56 – 1.0 μm) during the firework
450 event. The shift in mode to slightly larger particles during the firework event may be due to
451 increased coagulation sinks (Zhang et al., 2010) and secondary production (Retama et al., 2019).
452 An additional coarse peak (3.2 – 5.6 μm) observed after the firework event is mainly attributed
453 to sea salt constituents (e.g., Cl^- , Na^+) and likely unrelated to firework emissions aging and
454 processing. The mass contribution of the “others” to the total measured water-soluble mass
455 concentration decreased during the firework event to 4.3% from 12.5% before and 11.6% after
456 the firework event due to the prevalence of the ionic species (nss- SO_4^{2-} , K^+ , NO_3^- , Cl^- , Mg^{2+} , Na^+ ,
457 Ca^{2+} , and NH_4^+) discussed earlier (Table 1).

458

459 3.4 Enriched Tracers in Firework Emissions

460 Bulk mass concentrations of eighteen of the forty-one measured species were enriched during the
461 firework event by more than two times compared to the average of their bulk mass
462 concentrations before and after the firework event (Fig. 5). Enrichments for Cu (65.2), Sr (24.4),
463 succinate (19.4), Ba (18.2), K^+ (16.3), nss- SO_4^{2-} (9.8), Al (6.9), Pb (6.1), and maleate (5.3) were
464 highest (> 5) among the species measured (Fig.5). Potassium and nss- SO_4^{2-} together contributed
465 to 70.9% of the total measured species during the firework event (Table 1). However, Cu, Sr,
466 succinate, Ba, Al, Pb, and maleate contributed a total of only 2.14% to the total measured species
467 mass concentration. This reinforces the importance of looking at enrichments rather than
468 absolute mass concentrations for identifying which aerosol constituents are firework tracers.
469 Tracer metals in firework emissions were previously shown to contribute a small fraction
470 (~<2%) to total PM mass (Jiang et al., 2014).

471 Of the eighteen species with observed enrichments exceeding two (Fig. 5), only those which are
472 firework components and that are uninfluenced by secondary formation are considered tracers.
473 The identified fourteen firework tracers based on these criteria are as follows: Cu, Sr, Ba, K^+ , Al,
474 Pb, Mg^{2+} , Cr, Tl, Cl^- , Mn, Rb, Zn, and Ag. Copper gives the blue-violet color of fireworks, Sr
475 gives the red color, Ba and Tl makes the green flame, and Rb gives a purple color. Potassium and
476 Ag (as AgCNO or silver fulminate) are propellants, Al is fuel, and Pb provides steady burn and
477 is also used as an igniter for firework explosions. Chromium is a catalyst for propellants, Mg is a
478 fuel, and Mg^{2+} is a neutralizer or oxygen donor (U.S. Department of Transportation, 2013).
479 Manganese is either a fuel or oxidizer, and Zn is used for sparks (Licudine et al., 2012; Martín-
480 Alberca and García-Ruiz, 2014; Shimizu, 1988; Wang et al., 2007; Ennis and Shanley, 1991).
481 Metals are usually in the form of Cl^- salts in fireworks (Wang et al., 2007). In this study, the
482 enrichment of Cl^- during the firework event was found to be 3.7. Some of the identified tracer
483 metals are regulated and their detection is of concern. Magnesium is not recommended as a
484 firework component because it is sensitive to heat and can easily ignite in storage (Do et al.,
485 2012). Lead is highly toxic and thus regulated (Moreno et al., 2010) as its occurrence in



486 fireworks is not ideal. Although SO_4^{2-} , maleate (fuel), and NO_3^- (oxidant) were also enriched
487 more than two times during the firework event and are also firework components (Zhang et al.,
488 2019), they can be formed secondarily via gas-to-particle conversion processes (Yang et al.,
489 2014) and are not considered as firework tracers. Succinate is likewise formed secondarily and is
490 not considered a firework tracer (Wang et al., 2007).

491 Size-resolved enrichments (Fig. 5) were highest in the submicrometer range for most measured
492 species. This is consistent with past studies such as in Italy (Vecchi et al., 2008), Taiwan (Do et
493 al., 2012), and Spain (Crespo et al., 2012) where elemental concentrations due to pyrotechnics
494 increased in the submicrometer mode. The peak size differentiated enrichments of the first five
495 firework tracers Sr (45.08), Ba (57.82), K^+ (48.70), Al (18.75), and Pb (69.07) were in the 1.0 –
496 1.8 μm size range. Copper (49.85) peaked between 0.56 – 1.0 μm because it did not have valid
497 data for diameters exceeding 1.0 μm . Strontium and Ba had very high enrichments (254.40 and
498 195.84) from 0.1 – 0.18 μm due to very low concentrations before and after the firework event in
499 that size range. Enrichments of up to ~1000 (Crespo et al., 2012) for Sr and Ba have been
500 observed due to pyrotechnics, and both are known firework tracers (Kong et al., 2015).

501 The size-resolved enrichments of other notable species (Fig. 5 and Fig. S6) peaked at specific
502 size ranges between 0.32 – 1.8 μm : Mg^{2+} (18.93, 0.056 – 0.1 μm), Cr (14.37, 1.0 – 1.8 μm), Tl
503 (18.12, 0.56 – 1.0 μm), Cl^- (170.94, 0.32 – 0.56 μm), Mn (6.29, 1.0 – 1.8 μm), Rb (6.87, 1.0 –
504 1.8 μm), NO_3^- (7.26, 0.56 – 1.0 μm), Cs (6.28, 1.0 – 1.8 μm), Mo (4.15, 0.32 – 0.56 μm), Ti
505 (6.63, 0.32 – 0.56 μm), Co (17.94, 0.56 – 1.0 μm), and methanesulfonate (MSA) (6.66, 0.56 –
506 1.0 μm). Among all the measured water-soluble species, Cl^- had the highest size-resolved
507 enrichment, followed by Sr, Ba, K^+ , Pb, and Cu. This is expected because inorganic salts
508 comprise an enormous percentage of firework emissions (Martín-Alberca et al., 2016).

509

510 3.5 SEM-EDX

511 Five SEM images from the different stages (0.18 – 1 μm) of the MOUDI sampler with possible
512 firework influence are highlighted (Fig. 7). There were signs of nano-scale aggregation that were
513 chain-like and reminiscent of soot particles from pyrolysis and combustion (Pirker et al., 2020;
514 Pósfai et al., 2003; D'Anna, 2015) in all of the images, and especially distinct in the 0.1 – 0.18
515 μm (Fig. 4b) and 0.18 – 0.32 μm (Fig. 7c) stages. Images for larger sizes revealed relatively
516 larger particles appearing as a translucent crystal-shaped rectangle in the 0.32 – 0.56 μm image
517 (Fig. 7d), in addition to a capsule-shaped particle (Fig. 7e) and a cubic-shaped particle (Fig. 7f)
518 in the two 0.56 – 1.0 μm images. The presence of such non-spherical shapes including chain
519 aggregates points to the potential for particle collapse and shrinking associated with humidified
520 conditions as noted in past work (Shingler et al., 2016 and references therein).

521 The chemical composition of the blank Teflon substrate (Fig. 7a) was examined first by EDX to
522 determine the background signals before the actual samples were analyzed. The color intensity of



523 the element maps (Fig. S7) relates the concentration of the analyzed element relative to the
524 backscattered electron image (gray-scale) of the sample. The background substrate was
525 dominated by C, F, and Al (bright yellow, bright blue, and bright blue-green, respectively, in Fig.
526 S7-a1/a2/a3). Metallic elements were distributed in each of the five featured SEM images.
527 Molybdenum and K were present in all of the substrate stages (bright red in Fig. S7-
528 b3/b4/c3/c8/d7/d8/e6/e7/f6/f9). Other metals were also found in the different stages such as K,
529 Mg, Al, Ru, Pd, Ba, Hf, and Tl. The identified heavy metals in the particles are commonly used
530 in firework as fuel components, colorants, and oxidants (Singh et al., 2019). Potassium, Mg, Al,
531 Ba, and Tl are in the group of firework tracers that were already identified (Section 3.4 and Fig.
532 5) to have mass bulk concentration enrichments exceeding two. Molybdenum exhibited a
533 reduced mass bulk concentration enrichment of 1.93 (Fig. 5), but had size-resolved enrichments
534 between 1.21 and 4.15 (Fig. 6) in the substrate cut-outs analyzed for EDX. The cube-shaped
535 feature in the 0.56 – 1.0 µm substrate appears to be KCl because of the high color density of K
536 and Cl in the elemental maps (bright red and bright blue-green in Fig. S7-f6/f8) and because the
537 shape of KCl is cubic (Pirker et al., 2020). The crystal-shaped rectangle in the 0.32 – 0.56 µm
538 range appears to be enriched by Cl (bright blue-green in Fig. S7-d6). The same applies to the
539 capsule-shaped particle in 0.56 – 1.0 µm image (bright blue-green in Fig. S7-e5). The chloride
540 ion (Cl⁻) is a component of metal salts, usually in the form of ClO₄⁻ or ClO₃⁻ (Tian et al., 2014)
541 used to color fireworks (Shimizu, 1988).

542 These results of the sampled portions of the substrate stages are consistent with the results of the
543 size-resolved submicrometer enrichments measured by IC and ICP-QQQ (Section 3.4) for Mo,
544 K, Mg, Al, Ba, and Tl. Molybdenum was brightest red in the 0.32 – 0.56 µm image (Fig. S7-d8),
545 consistent with the highest enrichments (4.15 in Fig. 6) for that size range. Potassium was
546 brightest red in the 0.56 – 1.0 µm image (Fig. S7-e6/f6), consistent with highest enrichments
547 (33.04 in Fig. 6). Magnesium was brightest yellow from 0.32 – 1.0 µm (Fig. S7-d4/e3/f4),
548 consistent with highest enrichments (9.50 and 11.58 in Fig. 6). Aluminum had a high signal in
549 the blank Teflon substrate but also was brightest blue-green (Fig. S7-d5/e4/f5) in between 0.32 –
550 1.0 µm in the sample during the firework event, consistent with highest enrichments (9.22 and
551 13.32 in Fig. 6). Barium was detected by EDX between 0.56 – 1.0 µm (Fig. S7-f11 where its
552 enrichment was 12.39 (Fig. 6). Thallium was detected between 0.56 and 1.0 µm (Fig. S7-f13) by
553 EDX, where its enrichment was highest (18.12 in Fig. 6) as detected by ICP-QQQ. The
554 submicrometer metal salts due to fireworks can uptake water at high humidity (ten Brink et al.,
555 2018).

556

557 3.6 Hygroscopicity Analysis

558 As fireworks alter the chemical profile of ambient PM, we estimate how aerosol hygroscopicity
559 responded during fireworks relative to periods before and after. For reference, typical κ values
560 range from 0.1 to 0.5 for diverse air mass types such as urban, marine, biogenic, biomass
561 burning, and free troposphere (Dusek et al., 2010; Hersey et al., 2013; Shingler et al., 2016;



562 Shinozuka et al., 2009). AzadiAghdam et al. (2019) reported size-resolved values ranging from
563 0.02 to 0.31 using data from the same field site in Metro Manila but for a different time period
564 and without any firework influence (July – December 2018). They found the highest values to be
565 coincident with MOUDI stages with most sea salt influence (3.2 – 5.6 μm).

566 For this study, a bulk κ value is reported for the size range between 0.056 – 3.2 μm as noted in
567 Section 2.6, and subsequent references to composition data are for this size range. Kappa was
568 enhanced during the firework event (0.18) compared to before (0.11), due mostly to increased
569 contributions from K_2SO_4 and $\text{Mg}(\text{NO}_3)_2$ (Fig. 8a). More specifically, the volume fractions of
570 K_2SO_4 and $\text{Mg}(\text{NO}_3)_2$ increased from 0.01 to 0.10 and 0.01 to 0.03, respectively (Fig. 8b). For
571 context, inorganic salts (K_2SO_4 , KCl) dominated the aerosol hygroscopicity in Xi'an, China
572 during fireworks (Wu et al., 2018). In the Netherlands, enhancements in salt mixtures containing
573 SO_4^{2-} , Cl^- , Mg^{2+} , and K^+ were noted to enhance hygroscopicity (ten Brink et al., 2018). Notable
574 reductions in volume fraction during the firework event were for NaNO_3 (0.01 to 0.00), black
575 carbon (0.26 to 0.12), and $(\text{NH}_4)_2\text{SO}_4$ (0.02 to 0.01) (Fig. 8b). All three species are not
576 associated with primary firework emissions. Although NaNO_3 and $(\text{NH}_4)_2\text{SO}_4$ are hygroscopic,
577 their decreased volume fractions happened alongside a decreased volume fraction of non-
578 hygroscopic black carbon and increased volume fractions of the firework-related and
579 hygroscopic K_2SO_4 and $\text{Mg}(\text{NO}_3)_2$, which increased bulk aerosol hygroscopicity during the
580 firework event.

581 Kappa decreased to an intermediate value after the firework event (0.15) (Fig. 8a); this value
582 exceeds that from before the fireworks owing partly to more sea salt influence that was unrelated
583 to fireworks. The change in volume fraction of sea salt from before and during fireworks (0.01)
584 to after the fireworks (0.03) (Fig. 8b) translated to an increase of 0.03 in bulk κ (Fig. 8a) from
585 before to after the firework event. Although fireworks emit extensive amounts of inorganic
586 species, the calculated κ values were still relatively low because the background air is dominated
587 by organics and black carbon, which are relatively hydrophobic species (Table S4) (Cohen et al.,
588 2009; Oanh et al., 2006; Cruz et al., 2019).

589

590 4. Conclusion

591 This study reported on important aerosol characteristics measured during the 2019 New Year
592 fireworks in Metro Manila. Notable results of this work, following the order of questions raised
593 at the end of Section 1, are as follows:

594 • $\text{PM}_{2.5}$ was significantly enhanced during firework activities reaching a maximum of
595 383.9 $\mu\text{g m}^{-3}$ between 01:00 to 02:00 on 1 January 2019. Rainfall, wind, and relative
596 humidity possibly contributed to washout, local dispersion, and secondary formation of
597 particles, respectively. A noticeable decrease in aerosol backscatter was measured by the
598 HSRL lidar for short periods after the rain fall. There was no significant influence from
599 long-range transport to the sampling site, confirming that the sample data was most



600 representative of the local nature of particulate enhancements observed during the
601 firework event.

602 • Surface aerosol loading increased over a period of eight hours during the firework event,
603 coincident with peak PM_{2.5} levels. The heaviest aerosol layer was observed for at least an
604 hour, and reached ~440 m above the surface, after which the aerosol layer dropped to 118
605 ± 20 m.

606 • Bulk concentrations of water-soluble species were enhanced especially in the
607 submicrometer mode during the firework event along with increased water-soluble mass
608 fractions in PM_{2.5}. Potassium and nss-SO₄²⁻ were the major contributors. Mass size
609 distributions shifted to slightly larger accumulation-mode sizes most likely due to
610 increased coagulation sinks and secondary formation.

611 • Components of inorganic salts such as Cu, Sr, Ba, K⁺, Al, Pb, Mg²⁺, Cr, Tl, Cl⁻, Mn, Rb,
612 Zn, and Ag were enriched more than two times during the firework event as compared to
613 before and after the event. Even while they (excluding K⁺) comprised only 2.88% of the
614 total water-soluble mass, their contribution is significant because they support the
615 findings that the samples represent firework emissions, and especially since some of the
616 components like Pb and Mg²⁺ are banned substances.

617 • Cubic and capsule-shaped Cl⁻-rich particles, suggesting the presence of KCl, were
618 prominent in submicrometer particles collected during the firework event.

619 • Aerosol hygroscopicity (κ) between 0.056 and 3.2 μm increased from 0.11 (before the
620 fireworks) to 0.18 during the firework event due to the increased volume fractions of
621 inorganics.

622

623 The brief but sharply enhanced concentrations of water-soluble species in the submicrometer size
624 range, especially for K⁺ and SO₄²⁻, have implications for both public health and the environment,
625 the former of which is owing to how smaller particles can penetrate more deeply into the human
626 respiratory system. Higher concentrations of secondary particles from fireworks are related to
627 increased mass extinction efficiency and therefore decreased visibility (Jiang et al., 2014). The
628 increased water-soluble fraction during firework events coincides with elevated particle
629 hygroscopicity and CCN activity (Drewnick et al., 2006) at smaller diameters (Yuan et al.,
630 2020).

631

632 **Data availability**

633 High Spectral Resolution Lidar data collected at Manila Observatory can be found at:
634 (University of Wisconsin Lidar Group) http://hsrl.ssec.wisc.edu/by_site/30/custom_rti/

635 Size-resolved aerosols data collected at Manila Observatory can be found at: (Stahl et al., 2020a)
636 on figshare as well as on the NASA data repository at
637 DOI:10.5067/Suborbital/CAMP2EX2018/DATA001.



638

639 **Author Contributions**

640 MTC, MOC, JBS, RAB, ABM, CS, and AS designed the experiments. All coauthors carried out
641 various aspects of the data collection. MTC, EE, SV, RH, GL, LM, CS, and AS conducted
642 analysis and interpretation of the data. EE, LM, SV, RH, GL, and AS prepared the manuscript
643 with contributions from the coauthors.

644

645 **Competing Interests**

646 The authors declare that they have no conflict of interest.

647

648 **Acknowledgements**

649 The authors acknowledge support from NASA grant 80NSSC18K0148 in support of the NASA
650 CAMP²Ex project. R. A. Braun acknowledges support from the ARCS Foundation. M. T. Cruz
651 acknowledges support from the Philippine Department of Science and Technology's ASTHRD
652 Program. A. B. MacDonald acknowledges support from the Mexican National Council for
653 Science and Technology (CONACYT). We acknowledge Agilent Technologies for their support
654 and Shane Snyder's laboratories for ICP-QQQ data. We thank the Department of Environment
655 and Natural Resources Environmental Management Bureau (DENR-EMB) Central Office Air
656 Quality Management Section in the Philippines and the Air Center for Air Pollution Research in
657 Japan of EANET for the hourly PM_{2.5} data.

658

659 **References**

660 Agus, E. L., Lingard, J. J., and Tomlin, A. S.: Suppression of nucleation mode particles by
661 biomass burning in an urban environment: a case study, *Journal of Environmental Monitoring*,
662 10, 979-988, 2008.

663 Aldhaif, A. M., Lopez, D. H., Dadashazar, H., and Sorooshian, A.: Sources, frequency, and
664 chemical nature of dust events impacting the United States East Coast, *Atmospheric
665 Environment*, 117456, 2020.

666 Alpert, D. J., and Hopke, P. K.: A determination of the sources of airborne particles collected
667 during the regional air pollution study, *Atmospheric Environment* (1967), 15, 675-687, 1981.

668 Arimoto, R., Duce, R., Savoie, D., Prospero, J., Talbot, R., Cullen, J., Tomza, U., Lewis, N., and
669 Ray, B.: Relationships among aerosol constituents from Asia and the North Pacific during PEM-
670 West A, *Journal of Geophysical Research: Atmospheres*, 101, 2011-2023, 1996.

671 AzadiAghdam, M., Braun, R. A., Edwards, E.-L., Bañaga, P. A., Cruz, M. T., Betito, G.,
672 Cambaliza, M. O., Dadashazar, H., Lorenzo, G. R., and Ma, L.: On the nature of sea salt aerosol



673 at a coastal megacity: Insights from Manila, Philippines in Southeast Asia, *Atmospheric*
674 *Environment*, 216, 116922, 2019.

675 Barman, S., Singh, R., Negi, M., and Bhargava, S.: Ambient air quality of Lucknow City (India)
676 during use of fireworks on Diwali Festival, *Environmental monitoring and assessment*, 137, 495-
677 504, 2008.

678 Becker, J. M., Iskandrian, S., and Conkling, J.: Fatal and near-fatal asthma in children exposed to
679 fireworks, *Annals of Allergy, Asthma & Immunology*, 85, 512-513, 2000.

680 Beig, G., Chate, D., Ghude, S. D., Ali, K., Satpute, T., Sahu, S., Parkhi, N., and Trimbake, H.:
681 Evaluating population exposure to environmental pollutants during Deepavali fireworks displays
682 using air quality measurements of the SAFAR network, *Chemosphere*, 92, 116-124, 2013.

683 Braun, R. A., Dadashazar, H., MacDonald, A. B., Aldhaif, A. M., Maudlin, L. C., Crosbie, E.,
684 Aghdam, M. A., Hossein Mardi, A., and Sorooshian, A.: Impact of wildfire emissions on
685 chloride and bromide depletion in marine aerosol particles, *Environmental Science &*
686 *Technology*, 51, 9013-9021, 2017.

687 Braun, R. A., Aghdam, M. A., Bañaga, P. A., Betito, G., Cambaliza, M. O., Cruz, M. T.,
688 Lorenzo, G. R., MacDonald, A. B., Simpas, J. B., and Stahl, C.: Long-range aerosol transport
689 and impacts on size-resolved aerosol composition in Metro Manila, Philippines, *Atmospheric*
690 *Chemistry and Physics*, 20, 2387-2405, 2020.

691 Cao, Y., Zhang, Z., Xiao, H., Xie, Y., Liang, Y., and Xiao, H.: How aerosol pH responds to
692 nitrate to sulfate ratio of fine-mode particulate, *Environmental Science and Pollution Research*,
693 1-9, 2020.

694 Carranza, J., Fisher, B., Yoder, G., and Hahn, D.: On-line analysis of ambient air aerosols using
695 laser-induced breakdown spectroscopy, *Spectrochimica Acta Part B: Atomic spectroscopy*, 56,
696 851-864, 2001.

697 Chatterjee, A., Sarkar, C., Adak, A., Mukherjee, U., Ghosh, S., and Raha, S.: Ambient air quality
698 during Diwali Festival over Kolkata-a mega-city in India, *Aerosol and Air Quality Research*, 13,
699 1133-1144, 2013.

700 Cheng, Y., Engling, G., He, K.-b., Duan, F.-k., Du, Z.-y., Ma, Y.-l., Liang, L.-l., Lu, Z.-f., Liu,
701 J.-m., and Zheng, M.: The characteristics of Beijing aerosol during two distinct episodes:
702 Impacts of biomass burning and fireworks, *Environmental Pollution*, 185, 149-157, 2014.

703 Cohen, D. D., Stelcer, E., Santos, F. L., Prior, M., Thompson, C., and Pabroa, P. C.:
704 Fingerprinting and source apportionment of fine particle pollution in Manila by IBA and PMF
705 techniques: A 7-year study, *X-Ray Spectrometry: An International Journal*, 38, 18-25, 2009.

706 Crespo, J., Yubero, E., Nicolás, J. F., Lucarelli, F., Nava, S., Chiari, M., and Calzolai, G.: High-
707 time resolution and size-segregated elemental composition in high-intensity pyrotechnic
708 exposures, *Journal of hazardous materials*, 241, 82-91, 2012.

709 Crosbie, E., Sorooshian, A., Monfared, N. A., Shingler, T., and Esmaili, O.: A multi-year aerosol
710 characterization for the greater Tehran area using satellite, surface, and modeling data,
711 *Atmosphere*, 5, 178-197, 2014.

712 Cruz, M. T., Bañaga, P. A., Betito, G., Braun, R. A., Stahl, C., Aghdam, M. A., Cambaliza, M.
713 O., Dadashazar, H., Hilario, M. R., and Lorenzo, G. R.: Size-resolved composition and
714 morphology of particulate matter during the southwest monsoon in Metro Manila, Philippines,
715 2019.

716 D'Anna, A.: Kinetics of Soot Formation, 2015.



717 de Leeuw, G., Cohen, L., Frohn, L. M., Geernaert, G., Hertel, O., Jensen, B., Jickells, T., Klein,
718 L., Kunz, G. J., and Lund, S.: Atmospheric input of nitrogen into the North Sea: ANICE project
719 overview, *Continental Shelf Research*, 21, 2073-2094, 2001.

720 Devara, P. C., Vijayakumar, K., Safai, P. D., Made, P. R., and Rao, P. S.: Celebration-induced
721 air quality over a tropical urban station, Pune, India, *Atmospheric Pollution Research*, 6, 511-
722 520, 2015.

723 Do, T.-M., Wang, C.-F., Hsieh, Y.-K., and Hsieh, H.-F.: Metals present in ambient air before and
724 after a firework festival in Yanshui, Tainan, Taiwan, *Aerosol and Air Quality Research*, 12, 981-
725 993, 2012.

726 Dorado, S. V., Holdsworth, J. L., Lagrosas, N. C., Villarin, J. R., Narisma, G., Ellis, J., and
727 Perez, R.: Characterization of urban atmosphere of Manila with lidar, filter sampling, and
728 radiosonde, *Lidar Remote Sensing for Industry and Environment Monitoring*, 2001, 591-598.

729 Drewnick, F., Hings, S. S., Curtius, J., Eerdekens, G., and Williams, J.: Measurement of fine
730 particulate and gas-phase species during the New Year's fireworks 2005 in Mainz, Germany,
731 *Atmospheric Environment*, 40, 4316-4327, 2006.

732 Dusek, U., Frank, G., Curtius, J., Drewnick, F., Schneider, J., Kürten, A., Rose, D., Andreae, M.
733 O., Borrmann, S., and Pöschl, U.: Enhanced organic mass fraction and decreased hygroscopicity
734 of cloud condensation nuclei (CCN) during new particle formation events, *Geophysical Research
735 Letters*, 37, 2010.

736 Dutcher, D. D., Perry, K. D., Cahill, T. A., and Copeland, S. A.: Effects of indoor pyrotechnic
737 displays on the air quality in the Houston Astrodome, *Journal of the Air & Waste Management
738 Association*, 49, 156-160, 1999.

739 Ennis, J. L., and Shanley, E. S.: On hazardous silver compounds, *Journal of Chemical Education*,
740 68, A6, 1991.

741 Feng, J., Sun, P., Hu, X., Zhao, W., Wu, M., and Fu, J.: The chemical composition and sources
742 of PM_{2.5} during the 2009 Chinese New Year's holiday in Shanghai, *Atmospheric Research*,
743 118, 435-444, 2012.

744 Gysel, M., Crosier, J., Topping, D., Whitehead, J., Bower, K., Cubison, M., Williams, P., Flynn,
745 M., McFiggans, G., and Coe, H.: Closure study between chemical composition and hygroscopic
746 growth of aerosol particles during TORCH2, 2007.

747 Hersey, S. P., Craven, J. S., Metcalf, A. R., Lin, J., Lathem, T., Suski, K. J., Cahill, J. F., Duong,
748 H. T., Sorooshian, A., and Jonsson, H. H.: Composition and hygroscopicity of the Los Angeles
749 aerosol: CalNex, *Journal of Geophysical Research: Atmospheres*, 118, 3016-3036, 2013.

750 Hilario, M. R. A., Cruz, M. T., Bañaga, P. A., Betito, G., Braun, R. A., Stahl, C., Cambaliza, M.
751 O., Lorenzo, G. R., MacDonald, A. B., and AzadiAghdam, M.: Characterizing weekly cycles of
752 particulate matter in a coastal megacity: The importance of a seasonal, size-resolved, and
753 chemically-specified analysis, *Journal of Geophysical Research: Atmospheres*, e2020JD032614,
754 2020.

755 Hirai, K., Yamazaki, Y., Okada, K., FURUTA, S., and KUBO, K.: Acute eosinophilic
756 pneumonia associated with smoke from fireworks, *Internal medicine*, 39, 401-403, 2000.

757 Holz, R. E.: Measurements of cirrus backscatter phase functions using a high spectral resolution
758 lidar, *University of Wisconsin--Madison*, 2002.

759 Hooper, W. P., and Eloranta, E. W.: Lidar measurements of wind in the planetary boundary
760 layer: the method, accuracy and results from joint measurements with radiosonde and kytoon,
761 *Journal of climate and applied meteorology*, 25, 990-1001, 1986.



762 Hussein, T., Dal Maso, M., Petaja, T., Koponen, I. K., Paatero, P., Aalto, P. P., Hameri, K., and
763 Kulmala, M.: Evaluation of an automatic algorithm for fitting the particle number size
764 distributions, *Boreal environment research*, 10, 337, 2005.

765 Jiang, Q., Sun, Y., Wang, Z., and Yin, Y.: Aerosol composition and sources during the Chinese
766 Spring Festival: fireworks, secondary aerosol, and holiday effects, *ACPD*, 14, 20617-20646,
767 2014.

768 Joly, A., Smargiassi, A., Kosatsky, T., Fournier, M., Dabek-Zlotorzynska, E., Celo, V., Mathieu,
769 D., Servranckx, R., D'amours, R., and Malo, A.: Characterisation of particulate exposure during
770 fireworks displays, *Atmospheric Environment*, 44, 4325-4329, 2010.

771 Joshi, M., Khan, A., Anand, S., and Sapra, B.: Size evolution of ultrafine particles: Differential
772 signatures of normal and episodic events, *Environmental pollution*, 208, 354-360, 2016.

773 Joshi, M., Nakhwa, A., Khandare, P., Khan, A., and Sapra, B.: Simultaneous measurements of
774 mass, chemical compositional and number characteristics of aerosol particles emitted during
775 fireworks, *Atmospheric Environment*, 217, 116925, 2019.

776 Karnaee, S.: Analysis of aerosol composition and characteristics in a semi arid coastal urban area,
777 Texas A&M University-Kingsville, 2005.

778 Khaparde, V. V., Pipalatkar, P. P., Pustode, T., Rao, C. C., and Gajghate, D. G.: Influence of
779 burning of fireworks on particle size distribution of PM 10 and associated barium at Nagpur,
780 *Environmental monitoring and assessment*, 184, 903-911, 2012.

781 Kong, S., Li, L., Li, X., Yin, Y., Chen, K., Liu, D., Yuan, L., Zhang, Y., Shan, Y., and Ji, Y.: The
782 impacts of firework burning at the Chinese Spring Festival on air quality: insights of tracers,
783 source evolution and aging processes, *Atmos. Chem. Phys.*, 15, 2167-2184, 2015.

784 Kulshrestha, U., Rao, T. N., Azhaguvvel, S., and Kulshrestha, M.: Emissions and accumulation of
785 metals in the atmosphere due to crackers and sparkles during Diwali festival in India,
786 *Atmospheric Environment*, 38, 4421-4425, 2004.

787 Kumar, M., Singh, R., Murari, V., Singh, A., Singh, R., and Banerjee, T.: Fireworks induced
788 particle pollution: a spatio-temporal analysis, *Atmospheric research*, 180, 78-91, 2016.

789 Lai, Y., and Brimblecombe, P.: Changes in air pollution and attitude to fireworks in Beijing,
790 *Atmospheric Environment*, 117549, 2020.

791 Li, J., Xu, T., Lu, X., Chen, H., Nizkorodov, S. A., Chen, J., Yang, X., Mo, Z., Chen, Z., and
792 Liu, H.: Online single particle measurement of fireworks pollution during Chinese New Year in
793 Nanning, *Journal of Environmental Sciences*, 53, 184-195, 2017.

794 Licudine, J. A., Yee, H., Chang, W. L., and Whelen, A. C.: Hazardous metals in ambient air due
795 to New Year fireworks during 2004–2011 celebrations in Pearl City, Hawaii, *Public Health
796 Reports*, 127, 440-450, 2012.

797 Lin, C.-C.: A review of the impact of fireworks on particulate matter in ambient air, *Journal of
798 the Air & Waste Management Association*, 66, 1171-1182, 2016.

799 Lin, C.-C., Yang, L.-S., and Cheng, Y.-H.: Ambient PM2. 5, black carbon, and particle size-
800 resolved number concentrations and the Ångström exponent value of aerosols during the
801 firework display at the lantern festival in southern Taiwan, *Aerosol Air Qual. Res.*, 16, 373-387,
802 2016.

803 Liu, D.-Y., Rutherford, D., Kinsey, M., and Prather, K. A.: Real-time monitoring of
804 pyrotechnically derived aerosol particles in the troposphere, *Analytical Chemistry*, 69, 1808-
805 1814, 1997.



806 Marple, V., Olson, B., Romay, F., Hudak, G., Geerts, S. M., and Lundgren, D.: Second
807 generation micro-orifice uniform deposit impactor, 120 MOUDI-II: Design, evaluation, and
808 application to long-term ambient sampling, *Aerosol Science and Technology*, 48, 427-433, 2014.
809 Martín-Alberca, C., and García-Ruiz, C.: Analytical techniques for the analysis of consumer
810 fireworks, *TrAC Trends in Analytical Chemistry*, 56, 27-36, 2014.
811 Martín-Alberca, C., Zapata, F., Carrascosa, H., Ortega-Ojeda, F. E., and García-Ruiz, C.: Study
812 of consumer fireworks post-blast residues by ATR-FTIR, *Talanta*, 149, 257-265, 2016.
813 Mönkkönen, P., Uma, R., Srinivasan, D., Koponen, I., Lehtinen, K., Hämeri, K., Suresh, R.,
814 Sharma, V., and Kulmala, M.: Relationship and variations of aerosol number and PM10 mass
815 concentrations in a highly polluted urban environment—New Delhi, India, *Atmospheric*
816 *Environment*, 38, 425-433, 2004.
817 Mora, M., Braun, R. A., Shingler, T., and Sorooshian, A.: Analysis of remotely sensed and
818 surface data of aerosols and meteorology for the Mexico Megalopolis Area between 2003 and
819 2015, *Journal of Geophysical Research: Atmospheres*, 122, 8705-8723, 2017.
820 Moreno, T., Querol, X., Alastuey, A., Amato, F., Pey, J., Pandolfi, M., Kuenzli, N., Bouso, L.,
821 Rivera, M., and Gibbons, W.: Effect of fireworks events on urban background trace metal
822 aerosol concentrations: is the cocktail worth the show?, *Journal of hazardous materials*, 183, 945-
823 949, 2010.
824 Nicolás, J., Yubero, E., Galindo, N., Giménez, J., Castañer, R., Carratalá, A., Crespo, J., and
825 Pastor, C.: Characterization of events by aerosol mass size distributions, *Journal of*
826 *Environmental Monitoring*, 11, 394-399, 2009.
827 Oanh, N. K., Upadhyay, N., Zhuang, Y.-H., Hao, Z.-P., Murthy, D., Lestari, P., Villarin, J.,
828 Chenghua, K., Co, H., and Dung, N.: Particulate air pollution in six Asian cities: Spatial and
829 temporal distributions, and associated sources, *Atmospheric environment*, 40, 3367-3380, 2006.
830 Perrino, C., Tiwari, S., Catrambone, M., Dalla Torre, S., Rantica, E., and Canepari, S.: Chemical
831 characterization of atmospheric PM in Delhi, India, during different periods of the year including
832 Diwali festival, *Atmospheric Pollution Research*, 2, 418-427, 2011.
833 Perry, K. D.: Effects of outdoor pyrotechnic displays on the regional air quality of Western
834 Washington State, *Journal of the Air & Waste Management Association*, 49, 146-155, 1999.
835 Petters, M., and Kreidenweis, S.: A single parameter representation of hygroscopic growth and
836 cloud condensation nucleus activity, *Atmospheric Chemistry and Physics*, 7, 1961-1971, 2007.
837 Pirker, L., Gradišek, A., Višić, B., and Remškar, M.: Nanoparticle exposure due to pyrotechnics
838 during a football match, *Atmospheric Environment*, 117567, 2020.
839 Pósfai, M., Simonics, R., Li, J., Hobbs, P. V., and Buseck, P. R.: Individual aerosol particles
840 from biomass burning in southern Africa: 1. Compositions and size distributions of carbonaceous
841 particles, *Journal of Geophysical Research: Atmospheres*, 108, 2003.
842 Prospero, J. M., Savoie, D. L., and Arimoto, R.: Long-term record of nss-sulfate and nitrate in
843 aerosols on Midway Island, 1981–2000: Evidence of increased (now decreasing?) anthropogenic
844 emissions from Asia, *Journal of Geophysical Research: Atmospheres*, 108, AAC 10-11-AAC 10-
845 11, 2003.
846 Rao, P. S., Gajghate, D., Gavane, A., Suryawanshi, P., Chauhan, C., Mishra, S., Gupta, N., Rao,
847 C., and Wate, S.: Air quality status during Diwali Festival of India: A case study, *Bulletin of*
848 *environmental contamination and toxicology*, 89, 376-379, 2012.
849 Ravindra, K., Mor, S., and Kaushik, C.: Short-term variation in air quality associated with
850 firework events: a case study, *Journal of Environmental Monitoring*, 5, 260-264, 2003.



851 Razenkov, I.: Characterization of a Geiger-mode avalanche photodiode detector for high spectral
852 resolution lidar, University of Wisconsin--Madison, 2010.

853 Retama, A., Neria-Hernández, A., Jaimes-Palomera, M., Rivera-Hernández, O., Sánchez-
854 Rodríguez, M., López-Medina, A., and Velasco, E.: Fireworks: a major source of inorganic and
855 organic aerosols during Christmas and New Year in Mexico city, *Atmospheric Environment*: X,
856 2, 100013, 2019.

857 Rolph, G., Stein, A., and Stunder, B.: Real-time environmental applications and display system:
858 *READY*, *Environmental Modelling & Software*, 95, 210-228, 2017.

859 Santos, F. L., Pabroa, P. C. B., Morco, R. P., and Racho, J. M. D.: Elemental characterization of
860 New Year's Day PM10 and PM2. 2 particulates matter at several sites in Metro Manila, Book of
861 abstracts, 2007,

862 Sarkar, S., Khillare, P. S., Jyethi, D. S., Hasan, A., and Parween, M.: Chemical speciation of
863 respirable suspended particulate matter during a major firework festival in India, *Journal of*
864 *Hazardous Materials*, 184, 321-330, 2010.

865 Schlosser, J. S., Braun, R. A., Bradley, T., Dadashazar, H., MacDonald, A. B., Aldhaif, A. A.,
866 Aghdam, M. A., Mardi, A. H., Xian, P., and Sorooshian, A.: Analysis of aerosol composition
867 data for western United States wildfires between 2005 and 2015: Dust emissions, chloride
868 depletion, and most enhanced aerosol constituents, *Journal of Geophysical Research: Atmospheres*,
869 122, 8951-8966, 2017.

870 Shen, Z., Cao, J., Arimoto, R., Han, Z., Zhang, R., Han, Y., Liu, S., Okuda, T., Nakao, S., and
871 Tanaka, S.: Ionic composition of TSP and PM2. 5 during dust storms and air pollution episodes
872 at Xi'an, China, *Atmospheric Environment*, 43, 2911-2918, 2009.

873 Shimizu, T.: Fireworks: the art, science, and technique, Pyrotechnica publications, 1988.

874 Shingler, T., Crosbie, E., Ortega, A., Shiraiwa, M., Zuend, A., Beyersdorf, A., Ziembka, L.,
875 Anderson, B., Thornhill, L., and Perring, A. E.: Airborne characterization of subsaturated aerosol
876 hygroscopicity and dry refractive index from the surface to 6.5 km during the SEAC4RS
877 campaign, *Journal of Geophysical Research: Atmospheres*, 121, 4188-4210, 2016.

878 Shinozuka, Y., Clarke, A., DeCarlo, P., Jimenez, J., Dunlea, E., Roberts, G., Tomlinson, J.,
879 Collins, D., Howell, S., and Kapustin, V.: Aerosol optical properties relevant to regional remote
880 sensing of CCN activity and links to their organic mass fraction: airborne observations over
881 Central Mexico and the US West Coast during MILAGRO/INTEX-B, 1foldr Import 2019-10-08
882 Batch 9, 2009.

883 Singh, A., Pant, P., and Pope, F. D.: Air quality during and after festivals: Aerosol
884 concentrations, composition and health effects, *Atmospheric Research*, 2019.

885 Stahl, C., Cruz, M. T., Bañaga, P. A., Betito, G., Braun, R. A., Aghdam, M. A., Cambaliza, M.
886 O., Lorenzo, G. R., MacDonald, A. B., Pabroa, P. C., Yee, J. R., Simpas, J. B., and Sorooshian,
887 A.: An annual time series of weekly size-resolved aerosol properties in the megacity of Metro
888 Manila, Philippines, *Scientific Data*, 7, 128, 10.1038/s41597-020-0466-y, 2020b.

889 Stein, A., Draxler, R. R., Rolph, G. D., Stunder, B. J., Cohen, M., and Ngan, F.: NOAA's
890 HYSPLIT atmospheric transport and dispersion modeling system, *Bulletin of the American*
891 *Meteorological Society*, 96, 2059-2077, 2015.

892 Steinhauser, G., and Klapotke, T. M.: Using the chemistry of fireworks to engage students in
893 learning basic chemical principles: a lesson in eco-friendly pyrotechnics, *Journal of Chemical*
894 *Education*, 87, 150-156, 2010.

895 Stokes, R., and Robinson, R.: Interactions in aqueous nonelectrolyte solutions. I. Solute-solvent
896 equilibria, *The Journal of Physical Chemistry*, 70, 2126-2131, 1966.



897 Sun, Y., Wang, Z., Fu, P., Jiang, Q., Yang, T., Li, J., and Ge, X.: The impact of relative humidity
898 on aerosol composition and evolution processes during wintertime in Beijing, China,
899 *Atmospheric Environment*, 77, 927-934, 2013.

900 Tanda, S., Ličbinský, R., Hegrová, J., and Goessler, W.: Impact of New Year's Eve fireworks on
901 the size resolved element distributions in airborne particles, *Environment international*, 128, 371-
902 378, 2019.

903 ten Brink, H., Henzing, B., Otjes, R., and Weijers, E.: Visibility in the Netherlands during New
904 Year's fireworks: The role of soot and salty aerosol products, *Atmospheric Environment*, 173,
905 289-294, 2018.

906 Thakur, B., Chakraborty, S., Debsarkar, A., Chakrabarty, S., and Srivastava, R.: Air pollution
907 from fireworks during festival of lights (Deepawali) in Howrah, India-a case study, *Atmosfera*,
908 23, 347-365, 2010.

909 Tian, Y., Wang, J., Peng, X., Shi, G., and Feng, Y.: Estimation of the direct and indirect impacts
910 of fireworks on the physicochemical characteristics of atmospheric PM10 and PM2. 5,
911 *Atmospheric Chemistry and Physics*, 9469, 2014.

912 Totsuka, T., Sase, H., and Shimizu, H.: Major activities of acid deposition monitoring network in
913 East Asia (EANET) and related studies, in: *Plant Responses to Air Pollution and Global Change*,
914 Springer, 251-259, 2005.

915 Tsai, H.-H., Chien, L.-H., Yuan, C.-S., Lin, Y.-C., Jen, Y.-H., and Ie, I.-R.: Influences of
916 fireworks on chemical characteristics of atmospheric fine and coarse particles during Taiwan's
917 Lantern Festival, *Atmospheric Environment*, 62, 256-264, 2012.

918 Tsai, J.-H., Lin, J.-H., Yao, Y.-C., and Chiang, H.-L.: Size distribution and water soluble ions of
919 ambient particulate matter on episode and non-episode days in Southern Taiwan, *Aerosol and*
920 *Air Quality Research*, 12, 263-274, 2011.

921 Vecchi, R., Bernardoni, V., Cricchio, D., D'Alessandro, A., Fermo, P., Lucarelli, F., Nava, S.,
922 Piazzalunga, A., and Valli, G.: The impact of fireworks on airborne particles, *Atmospheric*
923 *Environment*, 42, 1121-1132, 2008.

924 Villafuerte II, M. Q., Matsumoto, J., Akasaka, I., Takahashi, H. G., Kubota, H., and Cinco, T. A.:
925 Long-term trends and variability of rainfall extremes in the Philippines, *Atmospheric Research*,
926 137, 1-13, 2014.

927 Walsh, K. J., Milligan, M., and Sherwell, J.: Synoptic evaluation of regional PM2. 5
928 concentrations, *Atmospheric Environment*, 43, 594-603, 2009.

929 Wang, Y., Zhuang, G., Xu, C., and An, Z.: The air pollution caused by the burning of fireworks
930 during the lantern festival in Beijing, *Atmospheric Environment*, 41, 417-431, 2007.

931 Wehner, B., Wiedensohler, A., and Heintzenberg, J.: Submicrometer aerosol size distributions
932 and mass concentration of the millennium fireworks 2000 in Leipzig, Germany, *Journal of*
933 *Aerosol Science*, 12, 1489-1493, 2000.

934 Wilkin, R. T., Fine, D. D., and Burnett, N. G.: Perchlorate behavior in a municipal lake
935 following fireworks displays, *Environmental Science & Technology*, 41, 3966-3971, 2007.

936 Williams, J., Drewnick, F., Hings, S. S., Curtius, J., Eerdekens, G., Klüpfel, T., and Wagner, T.:
937 Firework emissions for satellite validation?, *Environmental Chemistry*, 2, 94-95, 2005.

938 Wonaschuetz, A., Sorooshian, A., Ervens, B., Chuang, P. Y., Feingold, G., Murphy, S. M., De
939 Gouw, J., Warneke, C., and Jonsson, H. H.: Aerosol and gas re-distribution by shallow cumulus
940 clouds: An investigation using airborne measurements, *Journal of Geophysical Research:*
941 *Atmospheres*, 117, 2012.



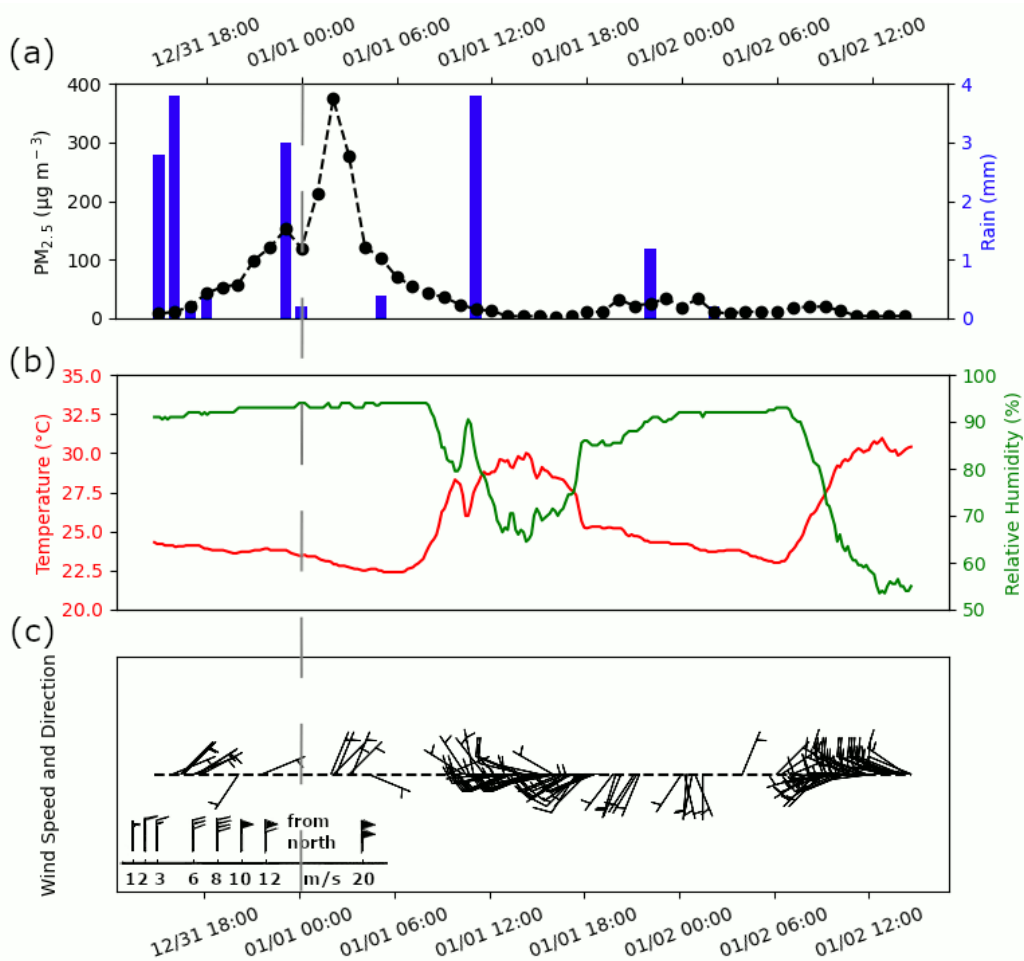
942 Wu, C., Wang, G., Wang, J., Li, J., Ren, Y., Zhang, L., Cao, C., Li, J., Ge, S., and Xie, Y.:
943 Chemical characteristics of haze particles in Xi'an during Chinese Spring Festival: Impact of
944 fireworks burning, *Journal of Environmental Sciences*, 71, 179-187, 2018.
945 Yadav, S. K., Kumar, M., Sharma, Y., Shukla, P., Singh, R. S., and Banerjee, T.: Temporal
946 evolution of submicron particles during extreme fireworks, *Environmental monitoring and*
947 *assessment*, 191, 576, 2019.
948 Yang, L., Gao, X., Wang, X., Nie, W., Wang, J., Gao, R., Xu, P., Shou, Y., Zhang, Q., and
949 Wang, W.: Impacts of firecracker burning on aerosol chemical characteristics and human health
950 risk levels during the Chinese New Year Celebration in Jinan, China, *Science of the Total*
951 *Environment*, 476, 57-64, 2014.
952 Youn, J. S., Wang, Z., Wonaschütz, A., Arellano, A., Betterton, E. A., and Sorooshian, A.:
953 Evidence of aqueous secondary organic aerosol formation from biogenic emissions in the North
954 American Sonoran Desert, *Geophysical research letters*, 40, 3468-3472, 2013.
955 Yuan, L., Zhang, X., Feng, M., Liu, X., Che, Y., Xu, H., Schaefer, K., Wang, S., and Zhou, Y.:
956 Size-resolved hygroscopic behaviour and mixing state of submicron aerosols in a megacity of the
957 Sichuan Basin during pollution and fireworks episodes, *Atmospheric Environment*, 226, 117393,
958 2020.
959 Zhang, J., Yang, L., Chen, J., Mellouki, A., Jiang, P., Gao, Y., Li, Y., Yang, Y., and Wang, W.:
960 Influence of fireworks displays on the chemical characteristics of PM2. 5 in rural and suburban
961 areas in Central and East China, *Science of the Total Environment*, 578, 476-484, 2017.
962 Zhang, J., Lance, S., Freedman, J. M., Sun, Y., Crandall, B. A., Wei, X., and Schwab, J. J.:
963 Detailed Measurements of Submicron Particles from an Independence Day Fireworks Event in
964 Albany, New York Using HR-ToF-AMS, *ACS Earth and Space Chemistry*, 3, 1451-1459, 2019.
965 Zhang, M., Wang, X., Chen, J., Cheng, T., Wang, T., Yang, X., Gong, Y., Geng, F., and Chen,
966 C.: Physical characterization of aerosol particles during the Chinese New Year's firework events,
967 *Atmospheric Environment*, 44, 5191-5198, 2010.



968 **Table 1:** Summary of total and speciated concentrations before, during, and after the firework
969 event. Species are divided based on units (Total to Zn: $\mu\text{g m}^{-3}$; succinate to Se: ng m^{-3}).

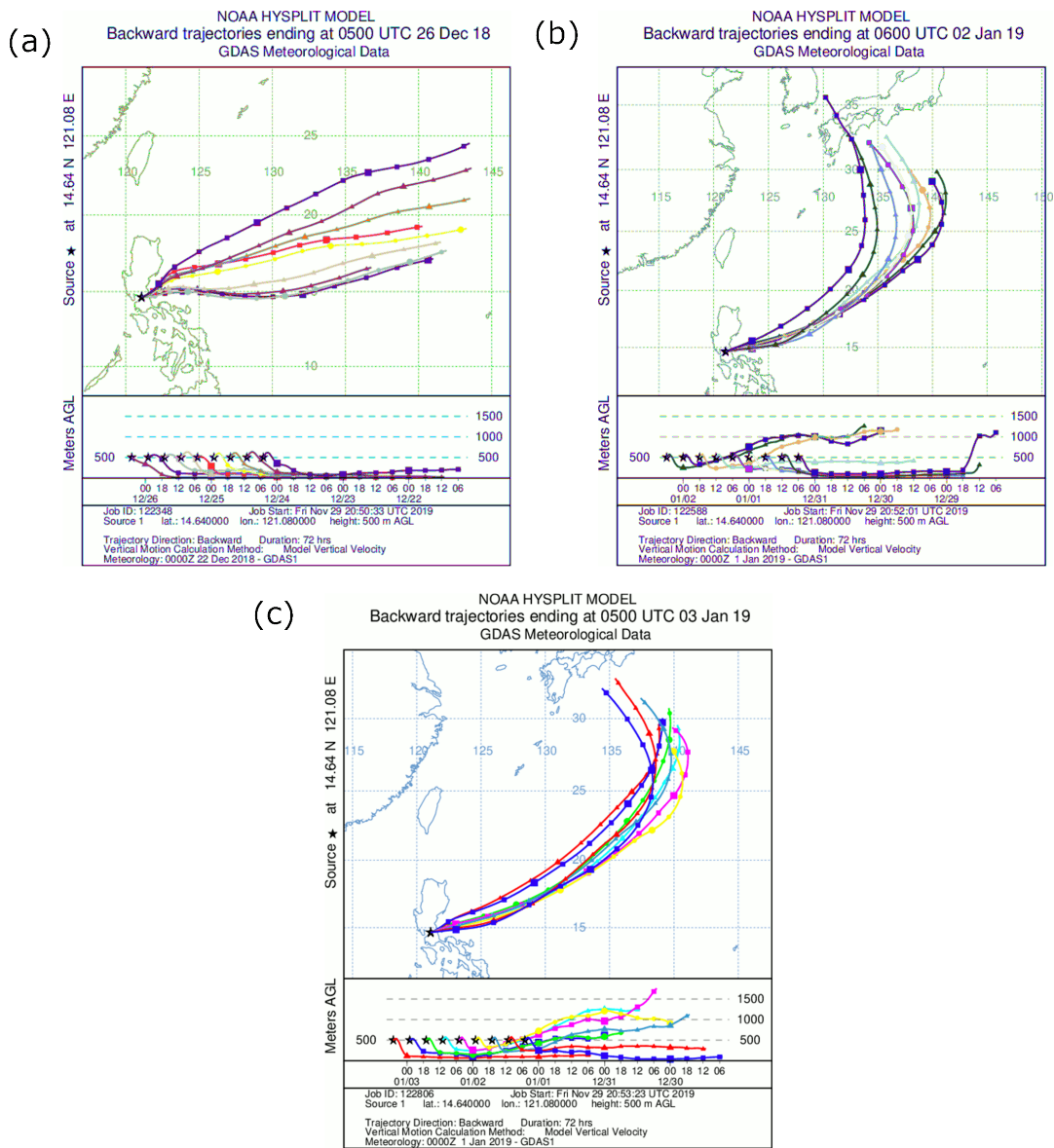
Species	Total Concentration			Species	Total Concentration		
	Before	During	After		Before	During	After
TOTAL	2.93	16.74	3.54	MSA	4.44	3.22	2.43
nss-SO₄²⁻	0.73	6.81	0.66	Mn	0.88	2.97	1.03
K⁺	0.37	5.05	0.25	Rb	0.62	1.24	0.25
NO₃⁻	0.64	1.70	0.65	Cr	0.16	1.01	0.29
Cl⁻	0.23	1.46	0.57	As	0.60	0.71	0.38
Mg²⁺	0.06	0.37	0.10	Ni	0.41	0.46	0.99
Na⁺	0.33	0.33	0.53	Ti	0.10	0.27	0.24
Ca²⁺	0.21	0.30	0.38	V	0.32	0.14	0.30
NH₄⁺	0.21	0.19	0.28	Mo	0.05	0.10	0.06
Ba	0.01	0.17	0.01	Cd	0.11	0.10	0.13
oxalate	0.10	0.12	0.06	Co	0.05	0.05	0.05
Cu	2.48E-04	6.89E-02	1.86E-03	Cs	0.02	0.02	0.01
Al	4.53E-03	0.05	0.01	Ag	0.02	0.02	4.00E-04
Sr	1.27E-03	4.65E-02	2.54E-03	Tl	0.01	0.02	1.80E-03
Zn	0.01	0.02	0.01	Zr	0.01	0.01	0.03
succinate	0.98	9.51	0	Sn	0.01	6.69E-04	0.03
Pb	1.68	8.33	1.03	Y	2.16E-04	4.56E-04	2.44E-03
phthalate	12.82	5.36	5.59	Nb	2.28E-04	1.59E-04	3.00E-04
adipate	5.35	4.83	11.73	Hf	0	0	2.18E-04
maleate	1.54	4.12	0	Hg	1.03E-03	0	0
Fe	2.91	3.47	7.32	Se	5.76	0	0

970



971

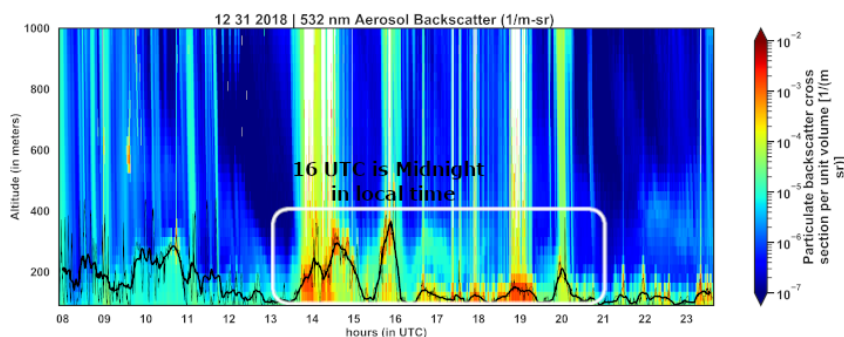
972 **Figure 1:** (a) PM_{2.5} mass concentrations and rain accumulation at hourly resolution (local time,
973 dashed vertical line indicates midnight) as measured from the Manila Observatory main building
974 third floor rooftop (~88 m.a.s.l.) at the same period as the MOUDI size-specified samples during
975 the firework event. Ten-minute averaged values of (b) temperature and relative humidity, in
976 addition to (c) wind speed and direction. The wind barb legend in (c) shows how flags are added
977 to the staff with increasing wind speed and in the direction where the wind comes from. Figures
978 S2 and S3 show the hourly PM_{2.5} mass concentrations and ten-minute meteorological data before
979 and after the firework event, respectively.



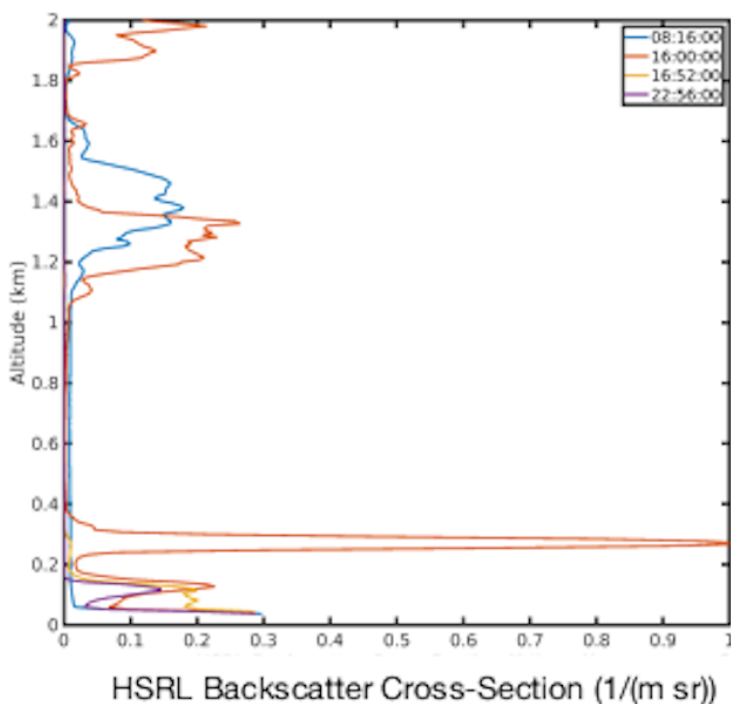
981 **Figure 2:** Three-day back trajectories with 6-h resolution for the periods (a) before, (b) during,
 982 and (c) after the firework event, ending at the point of the Manila Observatory at 500 m.



(a)



(b)



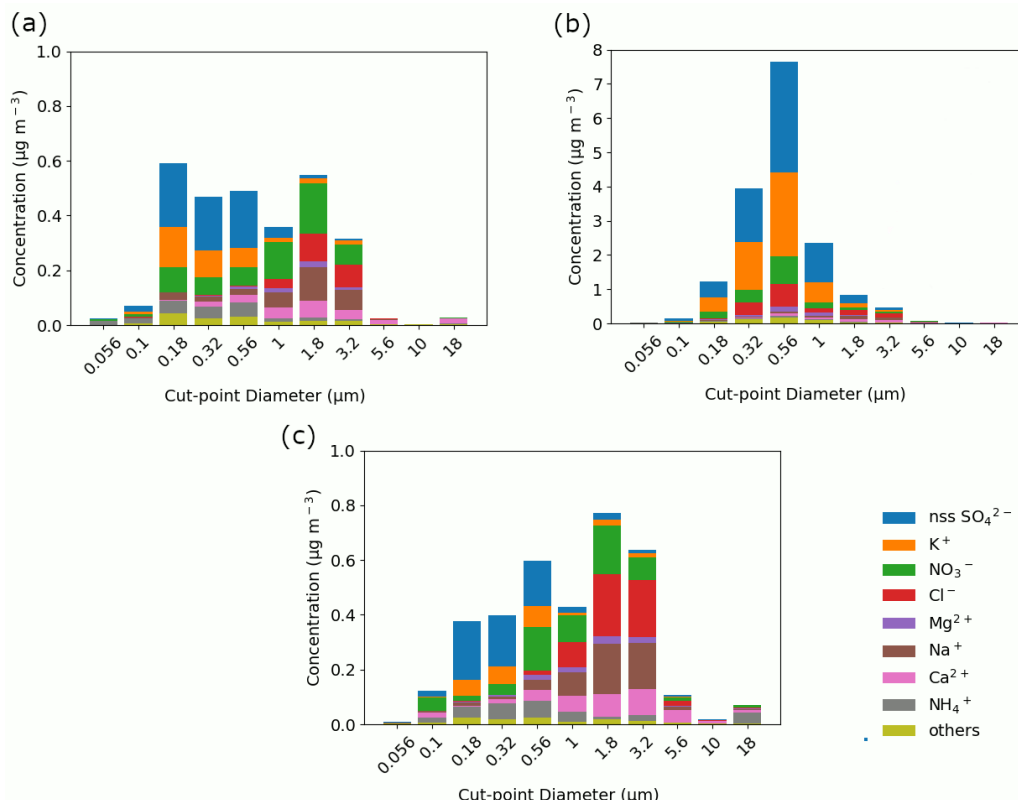
983

984 **Figure 3:** (a) Time series of the aerosol backscatter vertical profile from the High Spectral
985 Resolution Layer (HSRL). The time shown is Universal Time (UT) and local time is UT + 8
986 hours. The times circled by the white oval correspond to the peak of aerosol backscatter in the
987 mixing layer due to firework activity. The approximate surface-attached aerosol layer height is
988 shown as a thick black line. It is derived from a 30-min moving window average based on the 1-
989 min values shown in thin black line (b) Vertical profiles of aerosol back-scatter at specific UT
990 times of interest before, during, and after the fireworks.

991



992



993

994

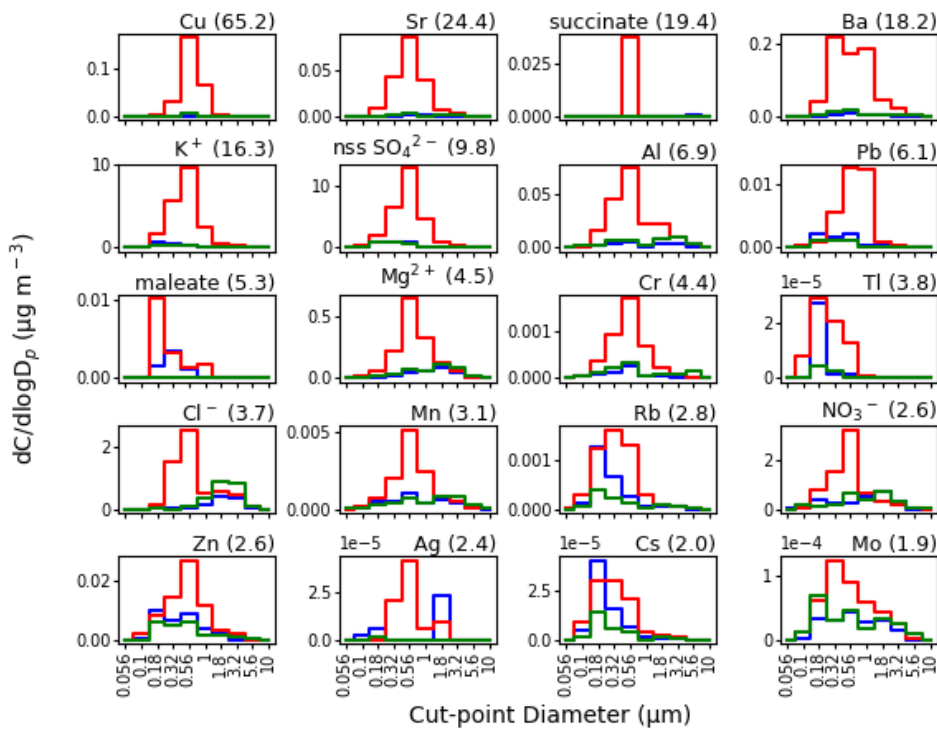
995

996

997

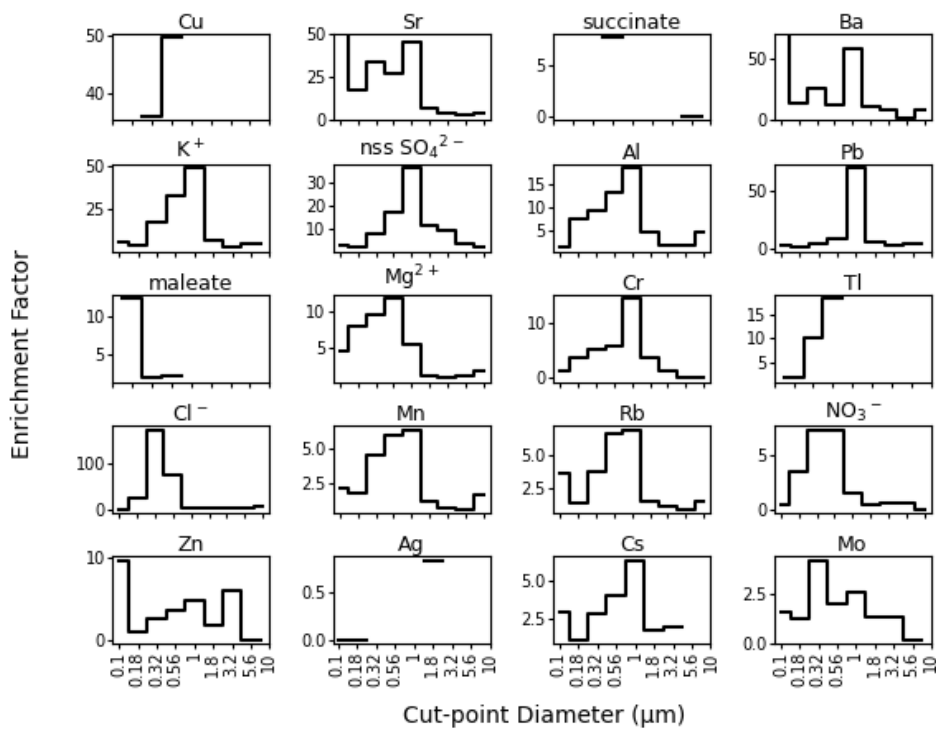
998

Figure 4: Speciated mass size distributions of the major aerosol constituents measured (a) before, (b) during, and (c) after the firework event. Table 1 lists the bulk ($\geq 0.056 \mu\text{m}$) mass concentrations of these ions and elements, including those labeled here as “others” (Ba, oxalate, Cu, Al, Sr, Zn, succinate, Pb, phthalate, adipate, maleate, Fe, MSA, Mn, Rb, Cr, As, Ni, Ti, V, Mo, Cd, Co, Cs, Ag, Tl, Zr, Sn, Y, Nb, Hf, Hg, and Se).



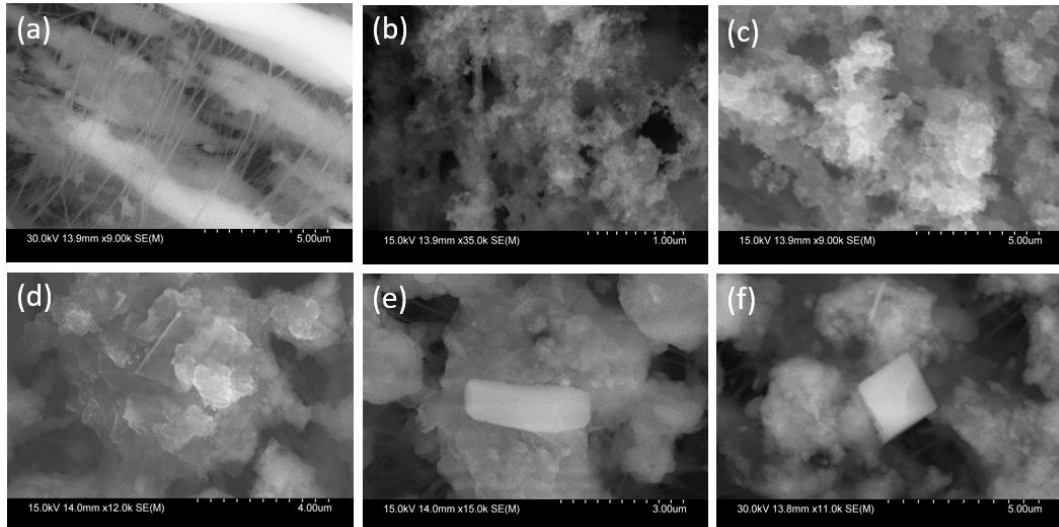
999

1000 **Figure 5:** Speciated mass size distributions before (blue line), during (red line), and after (green line) the firework event. Next to species labels are bulk ($\geq 0.056 \mu\text{m}$) mass concentration
1001 enrichment values due to the firework event; species are shown with enrichments ≥ 1.9 . Figure S5
1002 shows similar results for all other species.
1003



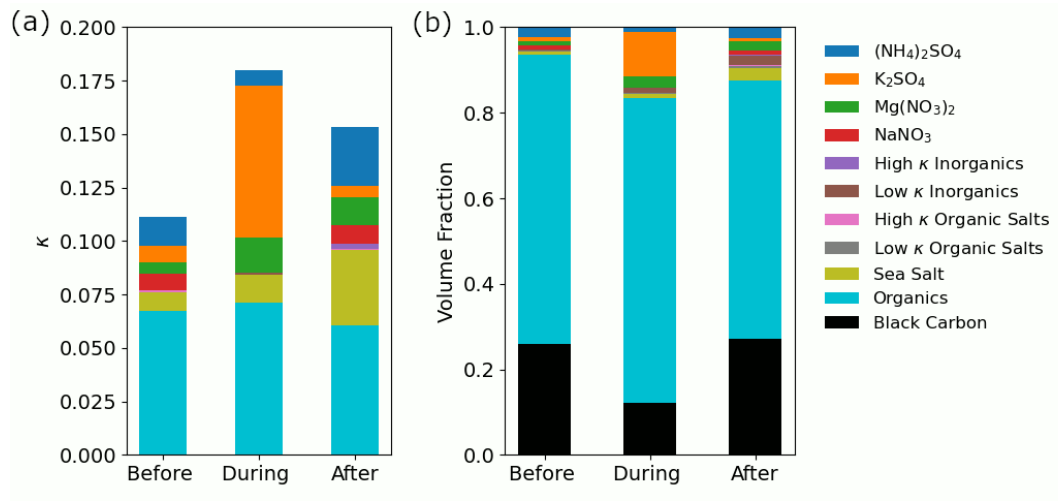
1004

1005 **Figure 6:** Size-resolved enrichments for individual firework tracer species in order of decreasing
1006 total bulk mass concentration enrichment (species from Fig. 5). Cut-point diameters with no
1007 valid data are left blank. The y-axis of Sr and Ba are truncated to more easily show enrichments
1008 in the larger size fractions. Figure S6 shows similar results for all other species.



1009

1010 **Figure 7:** Scanning electron microscope (SEM) images of (a) a blank PTFE (Teflon) substrate
1011 and (b-f) particles in different diameter ranges with firework influence: (b) 0.1 – 0.18 μm , (c)
1012 0.18 – 0.32 μm , (d) 0.32 – 0.56 μm , (e-f) 0.56 – 1.0 μm .



1013

1014 **Figure 8:** (a) Kappa (κ) values for the aerosol fraction between 0.056 – 3.2 μm before, during,
1015 and after the firework event. The speciated contributions to the overall κ values (represented by
1016 the colors) are categorized based on the classes of compounds in the legend following past work
1017 (AzadiAghdam et al., 2019). Ammonium sulfate, K_2SO_4 , $\text{Mg}(\text{NO}_3)_2$, and NaNO_3 are high κ
1018 inorganics but are plotted separately because of their large contributions. The speciated
1019 contributions were calculated by multiplying the volume fraction of each compound class by its
1020 intrinsic κ value (Table S4).